Chemical Geology 691 (2025) 122940

Contents lists available at ScienceDirect

Chemical Geology

journal homepage: www.elsevier.com/locate/chemgeo

Research Paper

Controls of sediment-bound and dissolved nutrient transport from a glacierised metasedimentary catchment in the high Arctic

Lukasz Stachnik [a,b,c,*], Jon Hawkings [c,d,**], Andrea Spolaor [e,f], Katarzyna Stachniak [g], Dariusz Ignatiuk [g], Sławomir Sitek [g], Krzysztof Janik [g], Elżbieta Łepkowska [g], Francois Burgay [h], Marcin Daniel Syczewski [b,i], Delia Segato [e,f], Pablo Forjanes [b], Liane G. Benning [b,j]

[a] University of Wrocław, Faculty of Earth Sciences and Environmental Management, Alfred Jahn Cold Regions Research Centre, Fryderyka Joliot-Curie Str. 12, 50-383 Wrocław, Poland
[b] GFZ, Helmholtz Centre for Geosciences, Potsdam, Telegrafenberg, 14473 Potsdam, Germany
[c] University of Pennsylvania, Department of Earth and Environmental Science, 251 Hayden Hall, 240 South 33rd Street, Philadelphia, USA
[d] iC3, Department of Geosciences, UiT, The Arctic University of Norway, Tromsø, Norway
[e] CNR-Institute of Polar Science (ISP), Campus Scientifico, Via Torino 155, 30172 Venice-Mestre, Italy
[f] Department of Environmental Sciences, Informatics and Statistics, Ca' Foscari University, Venice, Italy
[g] Institute of Earth Sciences, Faculty of Natural Sciences, University of Silesia in Katowice, Będzińska 60, 41-200 Sosnowiec, Poland
[h] Department of Environmental Sciences, University of Basel, 4056 Basel, Switzerland
[i] Faculty of Biology, University of Warsaw, Ilji Miecznikowa 1, 02-096 Warszawa, Poland
[j] Department of Earth Sciences, Freie Universität Berlin, 12249, Berlin, Germany

ARTICLE INFO

Editor: Dr. Don Porcelli

Keywords:
Glacier
Meltwater
Silica
iron
Arctic
Svalbard
Suspended sediments

ABSTRACT

Rapid warming in polar and alpine areas is causing significant glacier mass loss and resulting in increasing freshwater delivery to the oceans. Recent research indicates that higher meltwater water runoff is likely to increase solute and sediment transport, which will include nutrients, to downstream environments. This enhanced delivery may drive a negative feedback effect on atmospheric CO_2 concentrations by stimulating primary production in fjords and near-coastal regions. Labile sediment-bound nutrient species constitute a high proportion of the total nutrient yield from glacierised catchments, but studies that investigate their source and behaviour are sparse. Here we determine sediment-bound and dissolved nutrient (Si, Fe, P) delivery from a polythermal glacier in SW Spitsbergen. Suspended sediment and dissolved samples were collected from subglacial outflows and a downstream site. Our results show high spatial variability in chemical weathering processes resulting in differences in sediment-bound nutrient concentration. Sulphide oxidation and carbonate dissolution appear more important in a channelised system underlain by rocks metamorphosed in green schist facies, and silicate mineral weathering appears more important in smaller subglacial outflows underlain by rocks undergone intense metamorphism in amphibolite facies. Sediments from the channelised outlet have two times higher content of sediment-bound highly reactive iron (~0.29 % dry weight, hereafter d.w.) than the minor subglacial outflows. In contrast, sediment-bound amorphous silica (ASi) is almost double in the minor subglacial outflows compared to the channelised outlet (~0.17 % d.w. vs ~0.10 % d.w.). The yield of sediment-bound Fe and Si (2.3 and 1.3 10^3 kg km^{-2} yr^{-1}, respectively) was several times higher than the dissolved flux of those elements. Sediment-bound Fe yields were in the range of values noted previously for the Greenland Ice Sheet. Our data reinforces the critical role of sediment-bound nutrients on elemental cycling in glacierised basins of the high Arctic.

* Corresponding author at: University of Wrocław, Faculty of Earth Sciences and Environmental Management, Alfred Jahn Cold Regions Research Centre, Fryderyka Joliot-Curie Str. 12, 50-383 Wrocław, Poland.
** Corresponding author at: University of Pennsylvania, Department of Earth and Environmental Science, 240 South 33rd Street, Philadelphia, USA
E-mail addresses: lukasz.stachnik@uwr.edu.pl (L. Stachnik), hawkings@sas.upenn.edu (J. Hawkings), andrea.spolaor@unive.it (A. Spolaor), katarzyna.stachniak@us.edu.pl (K. Stachniak), dariusz.ignatiuk@us.edu.pl (D. Ignatiuk), slawomir.s.sitek@us.edu.pl (S. Sitek), krzysztof.janik@us.edu.pl (K. Janik), elzbieta.majchrowska@us.edu.pl (E. Łepkowska), francois.burgay@psi.ch (F. Burgay), delia.segato@unive.it (D. Segato), pablo.forjanes@gfz.de (P. Forjanes), liane.g.benning@gfz.de (L.G. Benning).

https://doi.org/10.1016/j.chemgeo.2025.122940
Received 13 September 2024; Received in revised form 28 May 2025; Accepted 15 June 2025
Available online 16 June 2025

1. Introduction

Glacier melt and physical erosion deliver large quantities of freshwater and nutrients to aquatic environments, impacting the downstream biogeochemical cycling of carbon and other elements (Milner et al., 2017; Robison et al., 2023; St. Pierre, K.A., et al., 2019). The delivery of nutrients can enhance biological activity, which can lead to atmospheric CO_2 consumption through photosynthesis in downstream freshwater and marine ecosystems. However, the impact of glacier recession on downstream biogeochemical cycling is still poorly understood due to a dearth of data, particularly in regions outside of the Greenland Ice Sheet.

Nutrient speciation, principally the distinction between dissolved and sediment-bound species, remains poorly studied in glacial meltwater. The majority of geochemical studies dealing with glacier meltwater have focused on chemical weathering using dissolved inorganic ions (Liu, 2023; Tranter and Wadham, 2013; Wadham et al., 2010b), or dissolved organic matter (Bhatia et al., 2013; Holt et al., 2021; Hood et al., 2015). These studies have found rates of chemical weathering strongly linked to glacier physical erosion rates (Anderson, 2005) and biological activity (Mitchell et al., 2013; Vinšová et al., 2022).

There have been suggestions of a strong pH/redox gradient from and among subglacial drainage systems and proglacial environments leads to rapid changes in weathering environments, in extremes from anoxic and low pH to oxic and high pH conditions (Deuerling et al., 2018; Graly et al., 2016). These environmental shifts change solubility levels and lead to precipitation of secondary weathering products (Crompton et al., 2015) that are often poorly crystalline phases (e.g., iron oxyhydroxides or amorphous silica). This, in turn, can lead to a decrease in solute concentration in the meltwaters (Hatton et al., 2019a; Hawkings et al., 2017; Hawkings et al., 2014). As a consequence, the overall rate of chemical weathering and export of nutrients from glacierised basins may be underestimated if only dissolved solid mass flux is taken into account (Crompton et al., 2015).

Studies dealing with sediment-bound nutrient cycling outside of the Greenland Ice Sheet have focused mostly on phosphorous (P). Phosphorous speciation was investigated in supraglacial streams and cryoconites (Mueller et al., 2001; Stibal et al., 2008), and in meltwaters from the Alps and the Arctic (Föllmi et al., 2009; Hodson et al., 2004). These studies suggest a close link between phosphorous mass flux and glacier cover (Eiriksdottir et al., 2015; Hood and Berner, 2009). Unlike sediment-bound phosphorous, sediment-bound iron and silicon have received much less attention outside of Greenland despite their potential impacts on primary production in polar regions (Hawkings et al., 2017; Koffman et al., 2021; Shoenfelt et al., 2017).

Most studies that assessed sediment-bound iron have focused on iron with low lability (Hodson et al., 2017; Mitchell and Brown, 2007) or iron present in more crystalline minerals (Poulton and Raiswell, 2002; Poulton and Raiswell, 2005; Raiswell et al., 2006). The ascorbate reagent targets only the most reactive iron phases, preferentially extracts surface-bound Fe^{2+} and freshly precipitated 2-line ferrihydrite (Hawkings et al., 2018a; Raiswell et al., 2010). These reactive iron phases have been shown to enhance growth of phytoplankton and limit primary production in part of global ocean (Shoenfelt et al., 2017; Wyatt et al., 2023).

Only recently have studies started to reveal the presence and reactivity of amorphous silica coatings and nanoaggregates on glacial flour (Hatton et al., 2019a; Hatton et al., 2019b; Hawkings et al., 2017). Most of these studies have been based on ice sheet meltwaters, however, some ASi concentration data also exist for Arctic and subarctic valley glaciers. These data include glaciers in Svalbard, Iceland and Alaska (Hatton et al., 2019b), and display a large range in concentrations (0.09–2.1 dry weight % ASi, hereafter % d.w.). Glaciers sampled in Svalbard displayed rather low ASi (~0.1 % d.w.) concentrations, but consist of only three data points at present (Hatton et al., 2019b).

The spatial distribution of chemical weathering processes in glacierised catchments, the causes for these differences, and the impacts of elemental export are also poorly understood. Most research has focused on the rate and temporal variations of chemical weathering under subglacial (Hodson et al., 2000; Tranter and Wadham, 2013; Wadham et al., 2010b; Sundriyal et al., 2024) and proglacial conditions (Cooper et al., 2002; Deuerling et al., 2018; Kristiansen et al., 2013). A limited number of studies have tried to determine how spatial variations in geology and glacier catchment cover impact chemical weathering reactions and nutrient availability (Pryer et al., 2020). Other studies dealing with sediment-bound nutrients have focused on plutonic, volcanic or high grade metamorphic bedrock geology (Hawkings et al., 2014; Pryer et al., 2020). For Svalbard, this is a big knowledge gap because no studies address the effect of metasedimentary rocks, which are common to large parts of Svalbard (Dallmann and Elvevold, 2015).

Future changes in glacierised basins outside of the Greenland or Antarctic ice sheets (e.g., Scandinavia, Svalbard, High Mountain Asia) are predicted to lead to glacier mass losses of up to 75 % (IPCC, 2019) in turn exposing over half of currently ice covered areas to areal weathering (Bosson et al., 2023). Thus, there is a pressing need to understand the role of glaciers on the biogeochemical cycling of crucial elements as they also impact CO_2 cycling (Shukla et al., 2023).

In this study we hypothesise that intense chemical weathering and glacier erosion in the subglacial drainage systems of small polythermal glaciers can enhance nutrient delivery to downstream environments. We present mass fluxes of sediment-bound and dissolved nutrients (Fe, Si, P) from a high Arctic glacier underlain by metasedimentary bedrocks, an environment that is underrepresented in present biogeochemical research. We also evaluate the spatial distribution of chemical weathering and impacts on nutrient concentrations in glacial meltwater streams.

2. Study area

Werenskioldbreen is a polythermal, land-terminating valley glacier in South Spitsbergen (Hagen et al., 1993; Jania, 1988). It covers 25.7 km^2 (2017) of a 44.1 km^2 drainage basin (Ignatiuk et al., 2022), with boundaries clearly delineated by the mountain ranges and the ice-cored terminal and lateral moraines. The glacier is, on average, 119 ± 13 m thick with a maximum thickness of 275 ± 7 m (Navarro et al., 2014). It consists of a cold ice surface layer that is 50–100 m thick with temperate ice below (Pälli et al., 2003). The glacier terminus is frozen to the bed and forms a fully cold-based zone that extends approximately 0.7–1.0 km up-glacier (Pälli et al., 2003). The glacier is currently retreating approximately 25 m per year (Ciężkowski et al., 2018). Based on surface mass balance studies, the glacier mass balance has been −0.23 m w.e. for the past decade (Ignatiuk et al., 2022). Werenskioldbreen drainage system has been modelled several times (Decaux et al., 2019; Grabiec, 2017; Pälli et al., 2003; Piechota et al., 2012). Subglacial outflows include a channelised outflow (S2 Kvisla) and minor outflows (S4 Black spring subartesian outflow, and S1 Angell). All streams intersect at Breelva River, which drains the whole basin toward a gauging station (S3 hydrometric station) situated at a gorge in the terminal moraine (Majchrowska et al., 2015) (Fig. 1).

2.1. Geological settings

The Werenskioldbreen glacier is located above a complex succession of Precambrian and Early Paleozoic metamorphic rocks (Hecla Hoek Formation). The deformation and metamorphism of this formation has been traditionally ascribed to the Caledonian orogeny, that consolidated the crystalline basement of Svalbard during the Devonian (Harland, 1997). The study area can be divided into two major tectonic units with different geological units located to the north and to the south of the Werenskioldbreen glacier. In the southern area there is an older complex amphibolite facies metamorphic volcano-sedimentary succession. These are the Isbjørnhamna (metasedimentary) and Eimfjellet (metavolcanic) groups (Czerny et al., 1992a; Majka et al., 2008). The Isbjørnhamna

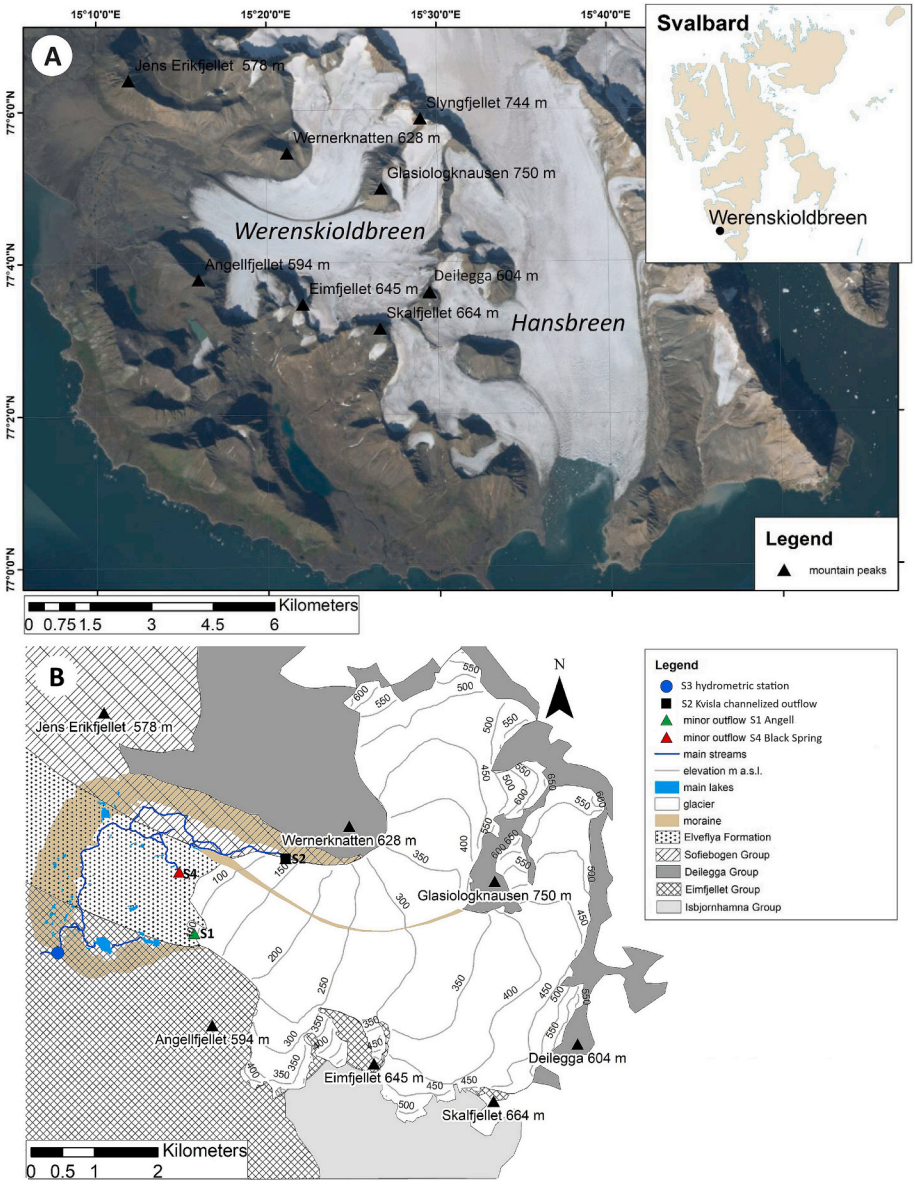

Fig. 1. Study area. A) location of Werenskioldbreen catchment, B) bedrock geology and sampling locations.

group consists mostly of micaschists and marbles, while the Eimfjellet Formation is dominated by quartzites, phyllites and amphibolites. These units underwent two metamorphic events spanning the amphibolite and greenschist facies. In the latter metamorphic episode there was extensive transformation of several of the metamorphic minerals into chlorite, as well as a destruction of numerous primary minerals such as plagioclase and dystene (Majka et al., 2008). These two formations are separated from the Deilegga and Sofiebogen units, to the north and more recent, by a tectonic contact with evidence of millonitisation. These two upper units underwent lighter metamorphism, in greenschist facies, and are dominated by conglomerates, carbonates and phyllites. The high content of metasedimentary carbonates in the upper units results in high carbonate content in the subglacial and proglacial sediments (Bukowska-Jania, 2003; Kwaśniak-Kominek et al., 2016). Sulphides (including chalcopyrite, pyrite, marcasite) were present in outcrop of the Hecla Hoek formation surrounding Werenskioldbreen (Czerny et al., 1992a; Kieres and Piestrzyński, 1992), and in the proglacial zone (Rzepa et al., 2019; Stachnik et al., 2019; Stachnik et al., 2022; Szynkiewicz et al., 2013). Gypsum has not been observed in the bedrock of Werenskioldbreen and is therefore not thought to contribute to the dissolved load of meltwaters in this catchment. The Werenskioldbreen glacier crosses the four major geological units of the Hecla Hoek Formation, including the tectonic contact between the two tectonic blocks. This results in an extremely complex geology capable of providing the system with varied rock-forming minerals.

3. Methods

3.1. Discharge measurements

The velocity-area method was used to determine discharge of the Breelva River (Fig. 1) as previously described (Majchrowska et al., 2015). Briefly, a rating curve was constructed based on ten representative discharge measurements ranging from 3.34 $m^3\ s^{-1}$ to 14.8 $m^3\ s^{-1}$ ($R = 0.83$) from June 14th to August 7th 2017. The measurements of water flow velocity were performed by an EM Flowmeter - Valeport model 801 equipped with flat sensor (accuracy of ±0.5 % of reading, range of velocity from - 5 to 5 m s^{-1}, minimal depth of measurement 5 cm). The average velocity was computed as the average of the one second real time values over the averaging period which has been set at

50 s. At the beginning of the ablation season (from June 14th to July 3rd 2017), discharge was reconstructed from direct measurements by flowmeter and SWAT model calibrated with SWAT-CUP software (version 5.1.6.2) (Gassman et al., 2007; Neitsch et al., 2011) due to the icing and snow in the river channel making installation of water level logger impossible. From July 4rd to September 27th 2017, water level was measured at 10 min intervals by a HOBO water level logger (model U20–001-04, with range 0–4 m and water level accuracy ±0.3 cm). An additional HOBO logger was installed in the Automatic Weather Station next to the Stanisław Baranowski Polar Station (SBPS) of the University of Wroclaw to compensate for atmospheric pressure. Runoff for entire season was calculated from sum of hourly runoffs based on average hourly discharge based on 10 min discharge values (calculated from rating curve).

3.2. Sampling campaign and physiochemical measurements

Water samples were collected from the hydrometric station (S3, $N = 45$), the major subglacial channelised outflow (S2 Kvisla outflow, $N = 7$), and two minor subglacial outflows (S1 Angell $N = 6$, and S4 Black Spring $N = 5$, hereafter minor outflows) (Fig. 1). Water at each site was sampled into two acid-washed 0.5 L HDPE (Nalgene™) bottles, which were pre-rinsed three times. Water was regularly sampled from the hydrometric station (usually two times per day), and less frequently from the subglacial outflows. The physiochemical properties of the sampled water were measured using a Hanna Instruments™ 9828 (resolution and accuracy in brackets, respectively): specific electric conductivity (1 μS cm^{-1} and ± 1 μS cm^{-1}, respectively), pH (0.01 pH and ± 0.02 pH, respectively), and water temperature (0.01 °C and ± 0.15 °C, respectively) were recorded, according to USGS protocols (Gibs et al., 2007).

Once returned to the field station, the water samples were immediately filtered via a glass vacuum filtration tower (Millipore™) with: 1) 0.7 μm pore size glass filters (Whatman™ GF/F) to evaluate the suspended sediment concentration (SSC), and 2) cellulose nitrate filters (Whatman™, 0.45 μm pore size) for water chemistry and to retain suspended sediments for chemical extractions. SSC samples were gently air-dried and, together with the filtered waters, kept in darkness at ~4 °C. Sediments for sequential extraction were gently removed from the filter and transferred to microcentrifuge tubes for storage.

3.3. Major ions chemistry

Major ion concentrations were determined by ion chromatography (Metrohm™ 850 Professional IC). Cations concentrations were measured using a Metrosep C4–150 column and using 0.7 mM dipicolinic acid /1.7 mM nitric acid as the eluent. Anions concentrations were measured using a Metrosep A-Supp 7–250/4.0 column and using 3.6 mM sodium bicarbonate as the eluent. Detection limits for analyses of Ca^{2+}, Mg^{2+}, Na^{+}, K^{+}, SO_4^{2-}, Cl^{-} and NO_3^{-} were 5.0 μeq L^{-1}, 8.0 μeq L^{-1}, 4.0 μeq L^{-1}, 3.0 μeq L^{-1}, 20.0 μeq L^{-1}, 30.0 μeq L^{-1} and 2.0 μeq L^{-1}, respectively. The certified reference materials NWRAIN-12 (lot 618) and NWCRANBERRY-05 (lot 618) were used to determine the accuracy and precision of analyses (Environmental and Climate Change Canada® LGC Standards®). Accuracy (as recovery) of analyses were between 98 and 113 % for most ions. Alkalinity was determined by titration using a Metrohm 702 SM Titrino with a glass pH electrode (Unitrode). Both the detection limit and the precision error of the alkalinity measurement were 10 μmol L^{-1}. Further error analyses are detailed in Appendix A (Eq. A.1).

3.4. Sediment-bound and dissolved nutrients analyses

Analyses of extracted sediment-bound and dissolved nutrient analyses (Si, Fe, P) were performed on suspended sediment samples from all stations spanning the range of discharges ($n = 25$ for Fe, and $n = 24$ for Si and P). Nutrients analyses were supplemented with mineralogical characterization determined by powder X-ray diffractometry (pXRD) and electron microscopic imaging (see details in section A.4. Mineralogical characterization of suspended sediments in Appendix A).

3.4.1. Highly reactive iron (Fe)

Highly reactive iron (assumed to be ferrihydrite nanoparticles and surface bound Fe(II)) as well as more crystalline iron (oxy)hydroxides (aged ferrihydrite, lepidocrocite, hematite and goethite) were extracted in ascorbic acid (FeA) and dithionite reagents (FeD; (Raiswell et al., 2018; Raiswell et al., 2010). Ascorbic acid, to a final concentration of 0.057 M, was added to a deoxygenated solution of 0.17 M sodium citrate and 0.6 M sodium bicarbonate, to create a buffered pH 7.5 ascorbic acid solution. The dithionite solution consisted of 50 g L^{-1} sodium dithionite in 0.35 M acetic acid and 0.2 M sodium citrate, buffered at pH 4.8. All reagents used were ACS grade or better. Approximately 30 mg of gently air-dried solid sample were accurately weighed into clean 15 mL PP centrifuge tubes (Falcon®). 10 mL of ascorbic acid solution was added and the mixtures placed onto a rotary shaker (150 rpm) at room temperature in the dark for 24 h. Subsequently, the samples were centrifuged at 10,000 rpm for 10 min and the supernatant filtered through a 0.22 μm PES syringe filter (Millex®) into clean 15 mL PP centrifuge tubes. The remaining solids were washed with 10 mL of ultra-pure water (UPW; Milli-Q, 18.2 MΩ cm^{-1}) for 10 min, before centrifuging and filtering the supernatant as above. In the second extraction step, the solids were mixed with 10 mL of the dithionite and again shaken at 150 rpm in the dark at room temperature for 2 h. The supernatants were filtered through a 0.2 μm syringe filter into clean 15 mL PP centrifuge tubes. Three blanks were treated the same as the samples. Ascorbic acid extracts were diluted 1:5 in UPW and dithionite extractions were diluted 1:25 in UPW. Total aqueous Fe was analysed via the ferrozine method after reduction with hydroxylamine (Viollier et al., 2000). Analyses were carried out on a Thermo Scientific™ Gallery™ discrete analyser with matrix-matched standards. The methodological limit of detection was below 250 nM. Precision was ±0.4 % and accuracy was - 2.5 %, calculated using a 50 μg L^{-1} (895 nM) gravimetrically made standard from a Fe(III) (using $FeCl_3$) standard stock.

3.4.2. Silica (Si)

Amorphous silica (ASi) concentrations were determined using a weak alkaline digestion (DeMaster, 1981), following methods previously employed for glacial suspended sediments (Hatton et al., 2019b; Hawkings et al., 2018b; Hawkings et al., 2017). This method is commonly used to determine biogenic opal in marine environments and amorphous silica in soils and fluvial sediments (Conley, 1998; Frings et al., 2014). Briefly, ~30 mg of air-dried suspended sediments were accurately weighed into clean 60 mL HDPE bottles (Nalgene™) and 50 mL of preheated 0.096 M sodium carbonate (ACS reagent grade) solution was added. Bottles were placed in a hot water bath set to 85 °C, and 1 mL aliquots were removed after 2, 3 and 5 h into clean 2 mL PP microcentrifuge tubes, using a calibrated 1 mL pipette. Aliquots were stored refrigerated for a maximum of 24 h before analysis. Before analysis, 0.5 mL of each aliquot was neutralised with 4.5 mL of 0.021 M HCl (ACS reagent grade). Samples were analysed for dissolved silicon on a LaChat QuikChem 8500 series 2 flow injection analyser (QuickChem method 31–114–27-1-D). The methodological limit of detection was 0.3 mM, precision ±0.7 % and accuracy +1.6 %. ASi concentration per unit mass of sediment was determined by using the intercept of a linear regression line through dissolved silica concentrations of 2, 3 and 5 h aliquots, assuming ASi dissolves rapidly within the first hour, and less reactive material (e.g., clays) dissolve at a slower, constant rate (DeMaster, 1981; Follett et al., 1965). The precision of the extractions was ±15.4 %, determined from two triplicate ASi measurements.

Dissolved silica (as silicic acid) was determined using the same method as extracts for amorphous silica (QuickChem method 31–114–27-1-D). Measurements were based on the molybdenum blue

method with addition of oxalic acid to minimise interference from phosphate. The methodological limit of detection was 0.3 μM, precision was ±1.3 % and accuracy was +2.1 %, as determined from five replicates of a 250 μg L^{-1} (8.9 μM) standard prepared by gravimetric dilution from a 1000 mg L^{-1} Si stock (CertiPur®).

3.4.3. Phosphorous (P)

Four operationally defined sediment bound phosphorus fractions were determined using a micro sediment extraction method developed and tested by Hawkings et al. (2016), a method that itself is a modified extraction after Hedley et al. (Hedley et al., 1982). Approximately 50 mg of air-dried suspended sediment samples were accurately weighed into clean 2 mL PP microcentrifuge tubes. Extraction were performed in four steps. Extraction step 1 removes highly labile, "loosely adsorbed" P with a 1 M magnesium chloride solution ($MgCl_2$-P). For extraction step 2, 1.5 mL of a 0.1 M sodium hydroxide (NaOH) solution was added to the previously extracted sediment to remove Fe- and Al- bound P (NaOH-P), which is moderately labile and sometimes referred to as "algal available" (Dorich et al., 1985). Extraction step 3 removes apatite bound (commonly referred to as Ca- and Mg- bound) P using 1.5 mL of a 1 M hydrochloric acid (HCl) solution (HCl-P). The final extraction (Extraction 4; Res—P) removes all remaining P, including organic bound-P fractions using a sulphuric acid (1 M)/potassium persulphate (0.22 M) solution. All extracts were kept refrigerated (<4 °C) until analysis, which was generally within 24 h. Solutions were analysed on a Thermo Scientific™ Gallery™ discrete analyser, using the molybdate-blue colorimetric method for soluble reactive phosphorus (EPA method 365.1). All reagents used were ACS grade or better. Samples were diluted in UPW before analysis at a ratio 1:3 ($MgCl_2$-P), 1:10 (NaOH-P), 1:100 (HCl-P), and 1:15 (Res—P). Precision for all extractions was < ± 2 % and accuracy was +10.3 %, + 1.3 %, + 6.4 % and − 3.1 % for extractions 1–4 respectively. This was based on replicate measurements of a gravimetrically weighed 50 μg L^{-1} matrix matched, diluted NIST-certified PO_4-P standard (TraceCERT®).

Soluble reactive phosphorus (SRP, also often referred to as dissolved inorganic phosphate) was determined on a LaChat QuickChem® 8500 series 2 flow injection analyser (FIA; QuickChem® Method 31–115–01-1-I). Measurements were based on the molybdenum blue method. Precision was ±3.2 % and accuracy was +1.5 %, as determined from five replicates of a 10 μg L^{-1} standard prepared by gravimetric dilution from a 1000 mg L^{-1} PO_4-P certified stock standard (Sigma TraceCERT®).

3.5. Nutrient fluxes and geochemical indices and statistical calculations

At the hydrometric station, mass fluxes of both sediment-bound nutrients and dissolved solids were calculated using discharge-weighted mean concentrations with suspended sediment flux and runoff from 2017. Suspended sediment mass flux was calculated based on discharge-weighted mean suspended sediment concentration and runoff. For dissolved Fe, mean values from an earlier study were used (Stachnik et al., 2019) as we did not make these measurements in our laboratory. To estimate the possible range of values, sediment-bound nutrient values include minimum and maximum measured concentrations in % d.w. (Hawkings et al., 2014). In addition, to further encapsulate a possible range for sediment-bound nutrient fluxes, suspended mass fluxes and runoff data from five ablation seasons (2007–2012) from earlier studies (Łepkowska and Stachnik, 2018; Majchrowska et al., 2015) were used.

Major ion concentrations (Ca^{2+}, Mg^{2+}, Na^{+}, K^{+}, SO_4^{2-}) were corrected for marine aerosol inputs (denoted as asterisk before a name of ion for $*Ca^{2+}$, $*Mg^{2+}$, $*SO_4^{2-}$ and ions for silicate weathering derived: Na_{sil}, K_{sil}) using the ratio between these ions and chloride in seawater (Eq. A.2; following (Hodson et al., 2000)) and sulphate mass fraction (SMF) coefficient was calculated. The sulfate mass fraction (SMF) is an indicator of chemical weathering used to distinguish sulfide oxidation, carbonation (dissolution of carbonate or silicate minerals by carbonic acid), and efflorescent salt dissolution (Eq. 1). A SMF equal to 0.5 corresponds to sulfide oxidation coupled to carbonate dissolution; SMF lower or higher than 0.5 indicates carbonation of carbonates and silicates or other processes are more dominant (sulfide oxidation coupled to silicate weathering, carbonate precipitation and Ca, Mg efflorescent salt dissolution), respectively (Cooper et al., 2002; Tranter et al., 2002).

$$SMF = \frac{*SO_4^{2-}}{*SO_4^{2-} + HCO_3^-} \quad (1)$$

where

SMF – sulfate mass fraction,

$*SO_4^{2-}$ – the concentration in μeq L^{-1} of sulfate, corrected for atmospheric input,

HCO_3^- – the concentration in μeq L^{-1} of bicarbonate.

Additional indices were calculated to determine the following processes: sea salt input (Cl:Na), sulphide oxidation ($*SO_4$:Na_{sil}), and ratio of silicate to carbonate weathering (K_{sil}:Na_{sil}, Ca_{carb}:Na_{sil}, Mg_{carb}:Na_{sil}, (Ca_{carb} + Mg_{carb}):(Ca_{sil} + Mg_{sil} + Na_{sil} + K_{sil}). The contribution of $*Ca^{2+}$ and $*Mg^{2+}$ originating from silicate (Ca_{sil}, Mg_{sil}, respectively) and carbonate (Ca_{carb}, Mg_{carb}, respectively) weathering was calculated according to Gaillardet et al. (1999). Further details are provided in Appendix 1 (Eqs. A.3-A.6).

To determine the strength of correlation between all parameters, non-parametric tests (Spearman's rank correlation, hereafter rho) were used. This correlation is resistant for non-normal distribution of variable and for outliers. Further, for selected relationship in the dissolved ion concentrations, linear regression fitting, Pearson correlation and determination coefficients (r, and r^2, respectively) were employed. Residual analysis (e.g., normal distribution and lack of autocorrelation) for these relationships was performed. For non-normally distributed residuals in the regression models, a logarithmic transformation of the variables was performed and regression model parameters (slope and constant term) were recalculated. All calculations were conducted using the Tibco Inc. ® Statistica software (ver. 13.3).

4. Results

4.1. Physiochemical water properties and suspended sediments

Water discharge was strongly linked to the physiochemical water properties at the hydrometric station (Fig. 2). Water discharge increased from ~4 m^3 s^{-1} in mid-June/early July to 16 m^3 s^{-1} at the peak flow in second part of July and then decreased to 4 m^3 s^{-1} by early August. Suspended sediment concentration (SSC) was on average ~ 770 mg L^{-1}, with the highest values at the water flow peak (1500 mg L^{-1}) and concentrations below 200 mg L^{-1} by early August. The diurnal pattern of suspended sediment mass flux was similar to that observed during earlier ablation seasons (2007–2008, 2010–2012, Fig. A.1). Water pH showed a similar trend to SSC, with slightly alkaline values up to mid-July and in the July/August (pH 7.8–8.4) but water with a pH ~9 during the peak flow. SSC was also strongly correlated with pH ($r > 0.7$, Fig. A.2).

Major ion concentrations decreased at all sites from early to peak flow, but the correlation between major ions remained strong. Mean concentrations for most major ions, including Ca^{2+}, Mg^{2+}, and SO_4^{2-}, decreased by a factor two or more from early season to the rising limb of hydrograph (14th – 19th July) (Fig. 3, Table A.1). HCO_3^- concentrations showed lower variability (640–976 μeq L^{-1}) with increasing concentrations up to the end of June and high variation during peak flow followed by a drop in concentration on the falling limb of the hydrograph. A strong correlation was observed between $*SO_4^{2-}$ (rho>0.85) and most major ions ($*Ca^{2+}$, $*Mg^{2+}$), while HCO_3^- was more poorly correlated (Table A.2). The relationship ($*Ca^{2+}$+$*Mg^{2+}$ vs. $*SO_4^{2-}$) had a slope close to ~1, a relatively high intercept value (700 μeq L^{-1}) and high correlation coefficient (Fig. 4A).

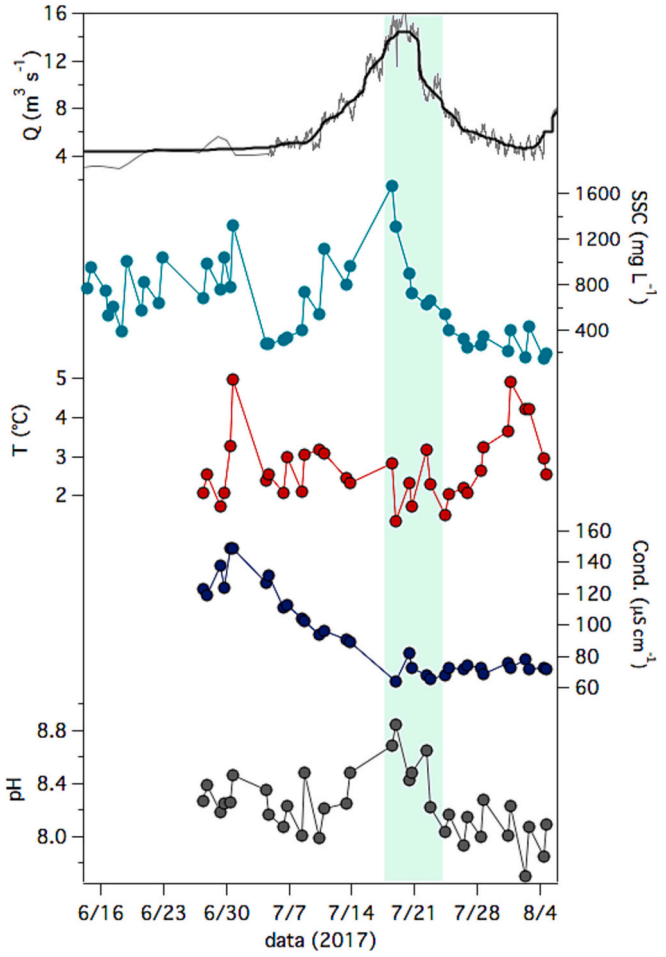

Fig. 2. Time resolved data for discharge (Q) and physiochemical water properties (pH, specific electric conductivity, water temperature, and suspended sediment concentration, SSC) acquired at the hydrometric station in the Werenskioldbreen during the summer melt season in 2017.

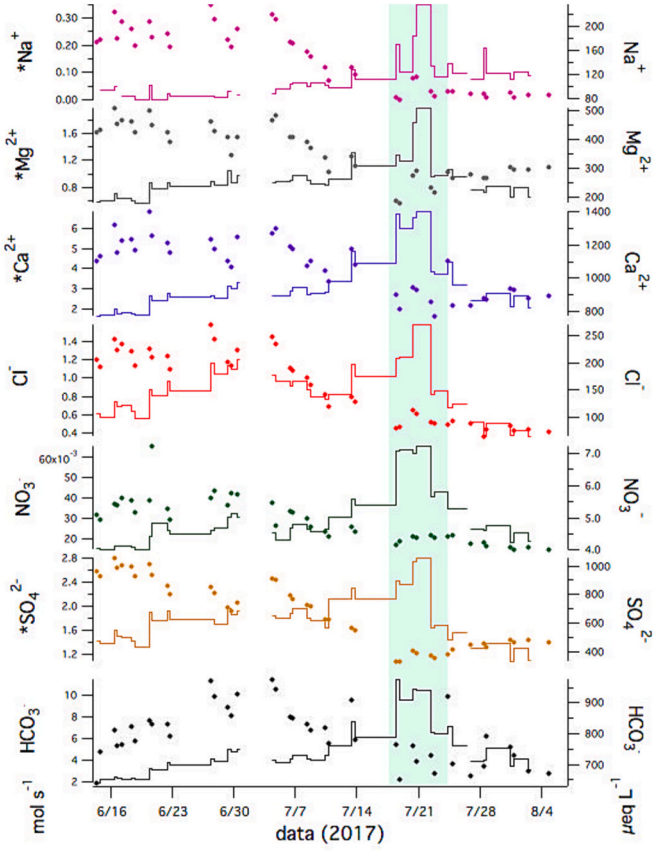

Fig. 3. Time resolved ion concentrations (points, right axis) and fluxes (lines, left axis) in the samples collected at the hydrometric station in Werenskioldbreen basin in the summer of 2017. Asterisks denote concentration corrected for atmospheric inputs (further details see Appendix A, Eq. A.2).

4.1.1. *Spatial distribution of indices and physiochemical properties in the catchment*

There was clear spatial variability in the physiochemical properties of water in the proglacial zone and between subglacial outflows (Table 1, Table A.1). Clear differences in indices such as SMF and the (Ca_{carb} + Mg_{carb}):(Ca_{sil} + Mg_{sil} + Na_{sil} + K_{sil}) ratio existed, the latter of which we use as a proxy for silicate vs carbonate mineral weathering (Table 1). Water from Kvisla (S2 channelised outflow) and the hydrometric station (S3) had a two-fold or higher SMF (0.44–0.46) than the smaller subglacial outflows (0.19, Fig. 4B S1 and S4), with similar patterns were observed for other indices (Table 1). The pH and specific electric conductivity of the minor subglacial outflows (S1 and S4) had high variability (pH 7.19–10.21, 21–65 µS cm^{-1}, respectively) and pH was generally lower than the Kvisla (Table A.1). Most major ions (HCO_3^-, SO_4^{2-}, Ca^{2+}, Mg^{2+}, Cl^-, F^- etc.) were higher in concentration in the Kvisla compared to the minor outflows (S1 and S4), apart from concentrations of Na^+ and K^+ which were higher in the minor outflows.

4.2. *Nutrient patterns and spatial distribution*

At the hydrometric station (S3), FeA and ASi con (% d.w.) were relatively stable throughout the ablation season (Tables 2 and 3). There was no correlation between discharge, FeA [% d.w.] and ASi [% d.w.] (Fig. 5, Table A.3), but SSC showed a negative correlation with ascorbate iron (rho = −0.88, Table A.3). All sediment-bound phosphorous concentrations were considerably lower (Table 4) than ASi and FeA. Despite a small decrease in ASi and FeA concentration (as % d. w.) (18th – 22nd July), the ASi and FeA water concentrations (µM) were highest at peak flow, up to ~50 µM for both ASi and FeA (Fig. A.3). Dissolved iron (0.57 µM based on earlier studies (Stachnik et al., 2019)), dissolved silicon (9.0 µM Table 3) and soluble reactive phosphorus (below detection limit of 0.04 µM) were on average ~ two orders of magnitude lower in concentration than their respective sediment-bound nutrients.

Sediment-bound nutrient concentrations exhibited large spatial differences (Fig. 6). The Kvisla, main subglacial outflow, had a higher FeA than both minor outflows (S1 and S4) (mean 0.29 % d.w., $N = 6$ vs. 0.12 % d.w., N = 6, respectively) (Table 2). Except the S1outflow, FeD (0.83–1.34 % d.w.) was similar between all sites with a large range of values for S4 and Kvisla (S2; Fig. A.4). ASi and sediment-bound phosphorous were significantly higher in % d.w. at the minor subglacial outflows than at Kvisla (channelised outflow, S2) and hydrometric station (S3; Tables 3–4). Suspended sediment concentration was highest in the Kvisla outflow (S3; average 934 mg L^{-1}) exceeding values from minor outflows (S1 and S4) by nearly an order of magnitude (Table A.1).

FeA and ASi showed strong correlations with the geochemical indices and physiochemical properties of the associated water samples (Fig. 7). While FeA was usually positively correlated with most major ions, ASi was mostly negatively correlated with them (Table A.3 A). Furthermore, FeA showed positive correlations with SMF (rho = 0.72 and rho = 0.49, respectively) and with the major ion ratio (Ca_{carb} + Mg_{carb}):(Ca_{sil} + Mg_{sil} + Na_{sil} + K_{sil}) (rho ~0.6). A linear regression model of FeA and SMF showed an exponential fit with a high coefficient of determination exceeding an $r^2 = 0.56$ (Fig. 7A). ASi (in % d.w.) was negatively correlated with SMF and (Ca_{carb} + Mg_{carb}):(Ca_{sil} + Mg_{sil} + Na_{sil} + K_{sil}) index (rho = −0.58 and rho = −0.52, respectively,

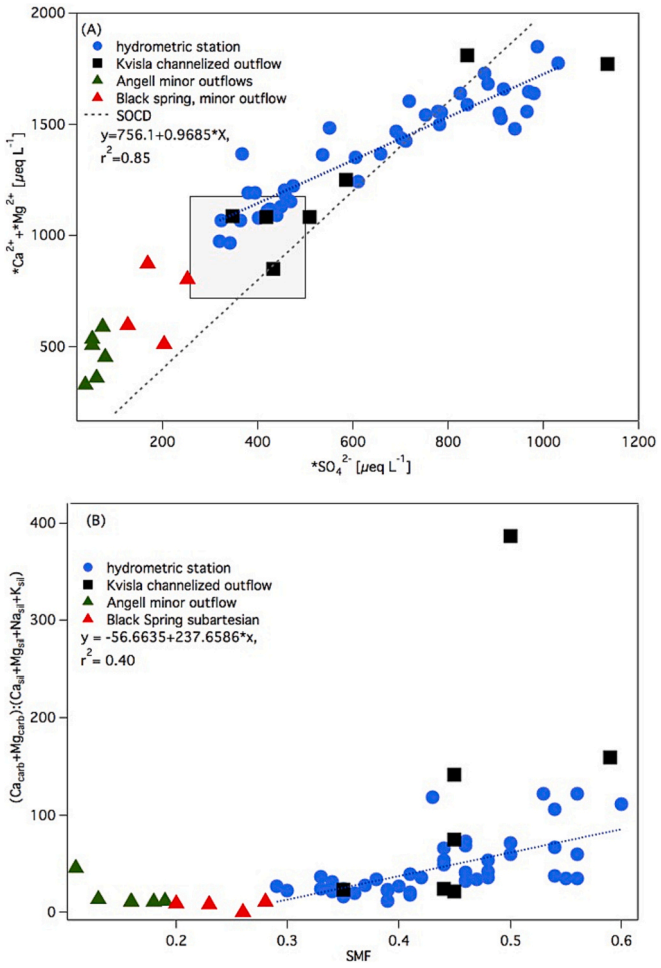

Fig. 4. Relationship between major ion ratios and sulfate concentrations (A) or sulfate mass fraction (SMF) (B) for S3 hydrometric station, minor outflows (S1 Angell outflow and S4 Black spring) and S2 Kvisla channelized outflow (see Fig. 1 for location of sites). Grey rectangle shows a range of concentrations observed for all subglacial outflow with evidence of sulphide oxidation (Szynkiewicz et al., 2020). SOCD is a theoretical line of sulphide oxidation coupled with carbonate dissolution.

Table A.3). A linear regression model indicated a negative linear relationship between ASi and SMF with a slightly lower coefficient of determination than FeA ($r^2 = 0.48$) (Fig. 7B). Both relationships fitted well with the spatial distribution of geochemical indices showing much higher SMF and $(Ca_{carb} + Mg_{carb})$:$(Ca_{sil} + Mg_{sil} + Na_{sil} + K_{sil})$ for Kvisla (S2) and the hydrometric station (S3) compared to minor outflows (Table 1).

4.3. Mineralogical analysis of the suspended sediments

There were variations in the mineral composition and abundance in sediments from the different study sites (Fig. 8). All samples contained four main phases: quartz, chlorite, micas and feldspars (~85 wt%). Site S1, located in the south of the Werenskioldbreen glacier (Fig. 1), is closest to the lower tectonic units (Isbjørnhamna and Eimfjellet groups), which underwent a higher degree of metamorphism. This explained why S1 samples had a high proportion of amphiboles, a mineral virtually absent in the sample obtained in S4. In contrast, suspended sediments of the S2 Kvisla site were high in goethite and contained minor amounts of siderite (~10 wt%). The sediments collected at hydrometric station (S3) also contain calcite and dolomite. SEM-EDS data showed good correlation with XRD data. The SEM data confirmed the presence of sulphides and traces of P were visible on iron oxides in sediments from Kvisla (S2; Fig. A.5) and possibly amorphous Si in sediments from Angell outflow (S1; Fig. A.5).

4.4. Mass fluxes of sediment-bound and dissolved nutrients and major ions

In 2017, specific runoff and suspended sediment mass flux were 1.72 m and 1280.65 10^3 kg km^{-2} yr^{-1}, respectively (Table A.4). Sediment-bound FeA 2.3 (1.9–3.7) 10^3 kg km^{-2} yr^{-1} and ASi 1.3 (1.0–1.8) 10^3 kg km^{-2} yr^{-1} mass fluxes were higher by factor of 42 and 3 compared to the dissolved Fe (0.05 10^3 kg km^{-2} yr^{-1}) and dissolved Si (0.41 10^3 kg km^{-2} yr^{-1}) fluxes respectively (Tables 2–3, Fig. 9). NaOH-P and total *P* values were from below detection limit and up to 0.708 10^3 kg km^{-2} yr^{-1}, respectively (Table 4).

5. Discussion

5.1. Major geochemical processes in the proglacial zone and subglacial outflows

Geochemical processes in the catchment displayed a clear switch during the transition from an inefficient distributed subglacial drainage system in late spring to a well-developed channelised efficient system in summer. A slope of $*Ca^{2+}$ and $*Mg^{2+}$ vs. $*SO_4^{2-}$ close ~1 (Cooper et al., 2002; Szynkiewicz et al., 2013) shows that multiple geochemical processes are controlling water chemistry composition, including sulphide oxidation and carbonate hydrolysis (Fig. 4, Figs. A.5 B and D). Sulphide oxidation has been shown to be occurring within subglacial system as evidenced by isotopic measurements of sulfur ($d^{34}S$) and oxygen ($d^{18}O$) in dissolved riverine sulfate from the Werenskioldbreen and other glacierised basins (Kemeny et al., 2021; Liu, 2023; Szynkiewicz et al., 2013). The switch in subglacial drainage pathways to more effective channelised drainage caused a sharp decrease in major ion concentration but an increase in solute mass flux due to the increase in discharge, with the highest mass flux observed during peak flow events (e.g., 19–21

Table 1
Geochemical indices calculated from the analysed ion concentrations in meltwaters from the Werenskioldbreen catchment during the ablation season 2017.

Geochemical indices	S1 Angell (N = 6)				S4 Black spring (N = 4)				S2 Kvisla channelized outflow (N = 7)				S3 hydrometric station (*N* = 42)			
	Mean	Median	Min	Max	Mean	Median	Min	Max	Mean	Median	Min	Max	Mean	Median	Min	Max
Cl:Na	1.0	1.0	0.9	1.1	0.8	0.8	0.4	1.0	1.1	1.1	0.9	1.8	1.1	1.1	0.7	1.3
$*SO_4$:Na_{sil}	14.0	6.8	5.1	52.2	6.5	5.9	1.3	12.9	72.6	38.1	19.8	149.1	616.5	60.8	13.8	14,191.6
Ca_{carb}:Na_{sil}	106.0	40.3	30.2	443.2	19.8	23.4	0.3	32.2	124.8	61.8	40.6	254.4	844.7	95.3	25.9	19,347.6
Mg_{carb}:Na_{sil}	8.0	8.1	7.2	8.7	4.4	4.3	1.8	7.2	34.9	17.8	12.8	68.8	274.7	29.5	7.3	6298.3
K_{sil}:Na_{sil}	2.6	2.0	1.0	7.4	0.8	0.9	0.4	1.2	0.6	0.4	0.0	1.6	9.8	1.3	0.4	207.8
$(Ca_{carb} + Mg_{carb})$: $(Ca_{sil} + Mg_{sil} + Na_{sil} + K_{sil})$	17.6	11.8	11.0	45.9	7.5	9.0	0.8	11.4	118.9	75.2	21.8	385.9	47.5	36.4	12.7	122.5
Sulphate mass fraction (SMF)	0.15	0.16	0.11	0.19	0.24	0.25	0.20	0.28	0.46	0.45	0.35	0.59	0.44	0.44	0.29	0.60

Table 2
Ascorbate (FeA) and dithionite iron (FeD) contents (in mean ± SD) extracted from the suspended sediments and calculated FeA mass fluxes from the Werenskioldbreen sampling locations compared with literature data from other glacierised basins. R denotes annual specific runoff.

Glacier	Geology	N	FeA [% d.w.]	FeA [μM]	FeD [% d.w.]	FeA [10^3 kg km^{-2} yr^{-1}]	R [m]	Reference
Werenskioldbreen (all sites)	Metasedimentary rocks carbonate-chlorite-quartz schists and calcareaous schists, phyllites, amphibolites	25	0.20 ± 0.09	17.3 ± 12.2	1.14 ± 0.13	2.3 (1.9–3.7)	1.72	This study
S3 hydrometric station		13	0.19 ± 0.04	20.7 ± 11.2	1.14 ± 0.10			This study
S2 Kvisla channelized outflow		6	0.29 ± 0.12	23.5 ± 10.1	1.13 ± 0.19			This study
minor outflows: S1 Angell and S4 Black spring		6	0.12 ± 0.02	3.57 ± 2.44	1.15 ± 0.16			This study
Leverrett Glacier	Orthogneisses/granite; Precambrian shield	33	0.15 ± 0.02		0.38 ± 0.06	5.8 (4.2–6.9)	3.67	Hawkings et al., 2014
Kiattuut Sermia	Granitic, with diorite−/pyroxene–biotite and basaltic intrusions; Precambrian shield	27	0.07 ± 0.02		0.22 ± 0.05			Hawkings et al., 2018
Russel Glacier	amphibolite and granulite facies gneisses, intermediate dykes	1	0.05		0.20			Yde et al., 2010
Patagonia*	diorites, quartz-diorites, tonalites, granodiorites, and monzogranite	32	0.31 ± 0.09		0.34 ± 0.01	0.97 (0.4–1.5)	5.63	Pryer et al., 2020
Greenland icebergs	Orthogneiss, possibly metasedimentary/ Metavolcanic; Precambrian shield	9	0.04 ± 0.01		0.34 ± 0.15			Hawkings et al., 2018
Svalbard icebergs	Metamorphosed basement rock (marbles/mica-schists), sandstones, shales, carbonates	9	0.13 ± 0.10		0.42 ± 0.21			Hawkings et al., 2018

* FeD is provided for Steffen Glacier in Patagonia only.

Table 3
Dissolved and amorphous silica content (DSi and ASi, in mean ± SD) in suspended sediments and yields from study area and other glacierised basins. Data from other regions are summarized in Pryer et al. (2020).

Site	DSi [μM]	ASi [% d.w.]	ASi [μM]	Yield DSi [10^3 kg km^{-2} yr^{-1}]	Yield ASi [10^3 kg km^{-2} yr^{-1}]	Source
Werenskioldbreen (all sites)	9.2 ± 2.3 (*N* = 58)	0.12 ± 0.03 (*N* = 24)	18.1 ± 13.5 (N = 24)	–	–	this study
S3 hydrometric station	9 ± 1.4 (*N* = 43)	0.10 ± 0.02 (*N* = 12)	22.1 ± 14.9 (N = 12)	0.41 (0.26–0.58)	1.3 (1.0–1.8)	this study
S2 Kvisla channelized outflow	8.7 ± 2.3 (N = 6)	0.10 ± 0.01 (N = 6)	20.2 ± 12.8 (N = 6)	–	–	this study
minor outflows: S1 Angell and S4 Black spring	10.7 ± 4.6 (*N* = 9)	0.17 ± 0.03 (*N* = 6)	8.1 ± 5.3 (N = 6)	–	–	this study
Other regions						
Greenland	25.4 ± 11.8	0.62 ± 0.35	202 ± 191	1.21 (0–2.5)	22 (9.6–34.4)	
Patagonia	32 ± 8.6	0.57 ± 0.08	12.0 ± 4.3	4.57 (2.27–6.87)	1.67 (0.68–2.66)	
Alaska	23.5 ± 8.5	0.39 ± 0.21		4.84 ± –	–	
Iceland	42.7 ± 32.8	1.04 ± 0.82		12.7 (10.4–15)	–	Summarized by Pryer et al. (2020)
Svalbard	3.8 ± 0.6	0.10 ± 0.02		0.23(0.12–0.34)	–	
Himalaya	44.5 ± 27.6	–		5.52 (1.11–9.93)	–	
Alps	27 ± 11	–		2 (1.49–2.51)	–	
Antarctica	29.2 ± 8.9	–		–	–	

July) (Fig. 4). This seasonal patterns of water chemistry is typical for glacierised basins and provides geochemical evidence of changes in subglacial drainage configuration and proglacial processes.

There is clear spatial variability in the geochemical processes occurring. Kvisla (S2 channelised outflow) in the northern part of the glacier has similar or slightly lower ion concentrations ($Ca_{carb} + Mg_{carb}$, $Na_{sil} + K_{sil}$, HCO_3^-) than the proglacial hydrometric station, as it is the main contributor to discharge at the hydrometric station (compared with minor tributaries sourced from S1 and S4) (Piechota et al., 2012). In the northern part of the catchment, metasedimentary bedrock and proglacial sediments enriched with carbonates (e.g., dolostones, calcareous schists, calcite marbles, (Bukowska-Jania, 2007; Czerny et al., 1992a); Fig. 8) were likely an additional source Ca^{2+}, Mg^{2+} and HCO_3^- at Kvisla. A high SMF (~0.4–0.5) and $*SO_4^{2-}$:Na_{sil} (19.8–149.1) at this site suggests that sulphuric acid produced via sulphide oxidation supplies protons for the dissolution of carbonates (Fig. A.5 B). In contrast, both average values of these indices are lower for the minor outflows S1 and S4 (SMF 0.15–0.24, $*SO_4^{2-}$:Na_{sil} 6.5–14). Dissolution of other SO_4 bearing minerals (e.g., gypsum, anhydrite) is unlikely a source as they are absent in bedrock (Czerny et al., 1992a; Czerny et al., 1992b), proglacial sediments (Bukowska-Jania, 2007; Kabala and Zapart, 2012), and suspended sediments (Stachnik et al., 2019).

The dissolution of silicate minerals (e.g., amphibolite, chlorite, biotite (Czerny et al., 1992a) in the southern and central parts of the catchment controls the chemical composition of water in the minor outflows (S1 and S4). S1 and S4 had considerably lower concentrations of carbonate weathering derived ions (Ca_{carb}, Mg_{carb}, and HCO_3^-) and higher concentration of ions and geochemical indices that typically indicate an increased prevalence of silicate weathering (e.g. high Na_{sil}, K_{sil}; low ($Ca_{carb} + Mg_{carb}$):($Ca_{sil} + Mg_{sil} + Na_{sil} + K_{sil}$), and low Ca_{carb}:Na_{sil} ratios). Sulphuric acid weathering of silicates is not likely to be important at these sites as the SMF (~0.15–0.24) and $*SO_4$:Na_{sil} is 511 times lower than Kvisla (S2; Table 1, Fig. 4). Other reactions driving silicate weathering in this part of glacier bed are likely to be carbonic

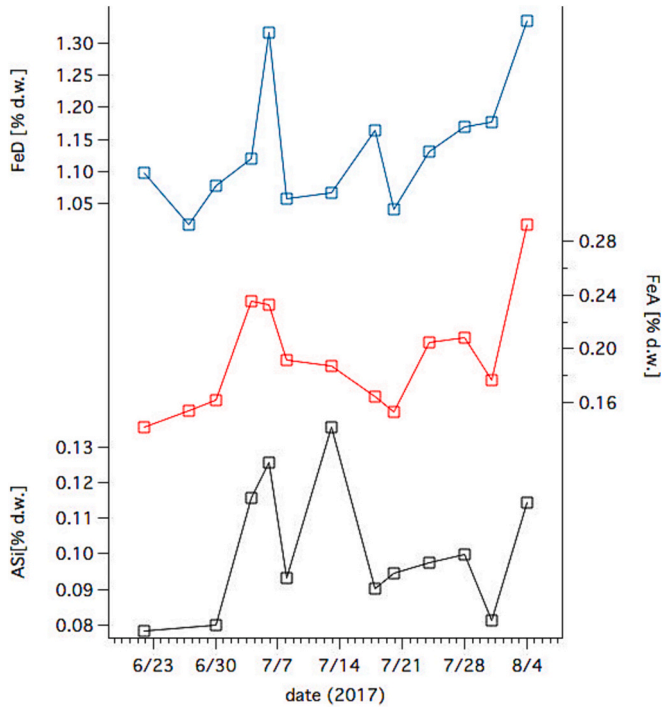

Fig. 5. Seasonal pattern of sediment-bound amorphous silica, ASi (bottom), ascorbate iron FeA (middle) and dithionite iron FeD (top) extracted form samples collected at the hydrometric station (S3, Fig. 1) in the Werenskioldbreen catchment during the ablation season 2017. Samples for sediment-bound nutrients analyses were selected from all collected samples to represent temporal variability, so their number is lower than in Fig. 3.

acid weathering or/and hydrolysis as water pH is neutral-alkaline (7.70–10.21) and HCO_3^- is approximately two times higher than SO_4^{2-} (Table A.1).

5.2. Processes affecting concentrations and transport of sediment-bound nutrients

Suspended sediment sampled from the channelised system (S2) and the hydrometric station (S3) has up to two times higher FeA (by % d.w.) compared to the minor outflows (S1 and S4). Major ion and geochemical indices indicate different geochemical conditions in the main channelised (S2) and the minor outflows (S1 and S4; see section 5.1 for further details), suggesting that geochemical processes occurring in the subglacial drainage system control the concentrations and therefore fluxes of sediment-bound Fe.

The channelised outflow (S2) drains a much larger area of the subglacial drainage system (~kilometre from the outflow) compared to minor outflows (<hundred meters from outflows)(Piechota et al., 2012). The larger catchment area could lead to a greater supply of water from more isolated up-catchment distributed systems. These more isolated systems will have higher solute content caused by long residence time, and high rock:water ratio. Iron sulphide (e.g. pyrite, marcasite) oxidation generating sulphuric acid (and consuming oxygen), would release dissolved Fe (both as Fe^{2+}/Fe^{3+}) to subglacial waters (Chillrud et al., 1994; Waychunas et al., 2005). When water from hypoxic distributed system mixes with oxygenated waters in the channelised subglacial drainage systems, the formation of poorly ordered iron (oxy)hydroxides (extractable as FeA) likely occurs. The presence of goethite in suspended sediment from S2 and S3 provides further evidence of iron sulphide transformation into secondary phases (Fig. 8 C). Carbonate dissolution coupled to sulphide oxidation neutralises the acidic pH and supports the formation of Fe oxyhydroxides. Microbial activity may also help facilitate the dissolution of Fe bearing mineral (and formation of Fe oxyhydroxides), as indicated by the occurrence of sulfur and iron oxidizing microbes (e.g., *Betaproteobacteria*, *Gammaproteobacteria*) (Sułowicz et al., 2020), but the efficiency of this process has not been determined.

FeD (more crystalline iron oxyhydroxides) was present at similar concentrations (% d.w.) between all sites (except S1 which was ~20 % lower on average) suggesting its formation may be affected by multiple processes, or that one predominant formation process occurs at all the sites. For example, sulphide oxidation is occurring (or has occurred) across the subglacial drainage (see section 5.1 for details). Additionally, the physical erosion of bedrock with abundant iron minerals (e.g., goethite, hematite (Kieres and Piestrzyński, 1992)) be a further explanation of similar FeD across sites.

Higher concentrations of FeA (0.20 ± 0.09 % d.w., Table 2) were found here compared with previous studies data from ice sheets. For example, glacial meltwater in Werenskioldbreen catchment has up to two times higher FeA and FeD by % d.w. than samples taken from Greenland (Hawkings et al., 2018a; Hawkings et al., 2014; Yde et al., 2010). When glaciers outside ice sheets underlain by more diverse bedrock (various igneous rocks) are considered, suspended particulate matter has a similar FeA to this study (up to 0.29 % d.w.) (Pryer et al., 2020). The FeA content at our sample area glacial flour is up to ~5 times higher that of iceberg rafted sediments from Greenland (Raiswell et al.,

Table 4
Proportion of various phosphorous fractions that wer sequentially extracted from the suspended sediments (in mean ± SD) and calculated yields from study area and other glacierised basins. Phosphorous concentration in extract 1 ($MgCl_2$) was below detection for all suspended sediment samples from Werenskioldbreen.

Study area	N	NaOH-P	HCl-P	Res-P/POP	PT	NaOH-P	PT	Source
		[% d.w.]				Yield (10^3 kg km^{-2} yr^{-1})		
Werenskioldbreen (all sites)	24	$1.60 \pm 3.52\ 10^{-4}$	$5.85 \pm 1.64\ 10^{-2}$	$4.08 \pm 0.74\ 10^{-3}$	$6.27 \pm 1.72\ 10^{-2}$	–	–	this study
S3 hydrometric station	13	$0.33 \pm 0.06\ 10^{-4}$	$5.24 \pm 0.49\ 10^{-2}$	$3.78 \pm 0.31\ 10^{-3}$	$5.63 \pm 0.47\ 10^{-2}$	<0.001	0.708	
S2 Kvisla channelized outflow	6	$0.99 \pm 0.93\ 10^{-4}$	$5.20 \pm 0.23\ 10^{-2}$	$3.80 \pm 0.74\ 10^{-3}$	$5.59 \pm 0.27\ 10^{-2}$	–	–	
minor outflows: S1 Angell and S4 Black spring	5	$5.60 \pm 6.67\ 10^{-4}$	$8.19 \pm 2.46\ 10^{-2}$	$5.18 \pm 0.49\ 10^{-3}$	$8.77 \pm 2.53\ 10^{-2}$	–	–	
Other glacierised basins								
Leverett Glacier	25	$14.6 \pm 7.5\ 10^{-4}$	$8 \pm 0.9\ 10^{-2}$	$3.4 \pm 0.75\ 10^{-3}$	$8.49 \pm 0.97\ 10^{-2}$	0.057	3.252	Hawkings et al. (2016)
Kiattut Sermiat	25	$11.9 \pm 3.2\ 10^{-4}$	$11.75 \pm 0.11\ 10^{-2}$	$2.19 \pm 0.37\ 10^{-3}$	$12.09 \pm 1.11\ 10^{-2}$	0.008	0.859	Hawkings et al. (2016)
Austre Broggerbreen	11	$3.5 \pm 2.4\ 10^{-4}$	–	–	$4.0\ 10^{-2}$	<0.001	0.064	Hodson et al. (2004)
Midre Lovenbreen	34	$2.5 \pm 1.5\ 10^{-4}$	–	–	$4.6\ 10^{-2}$	0.008	2.000	Hodson et al. (2004)

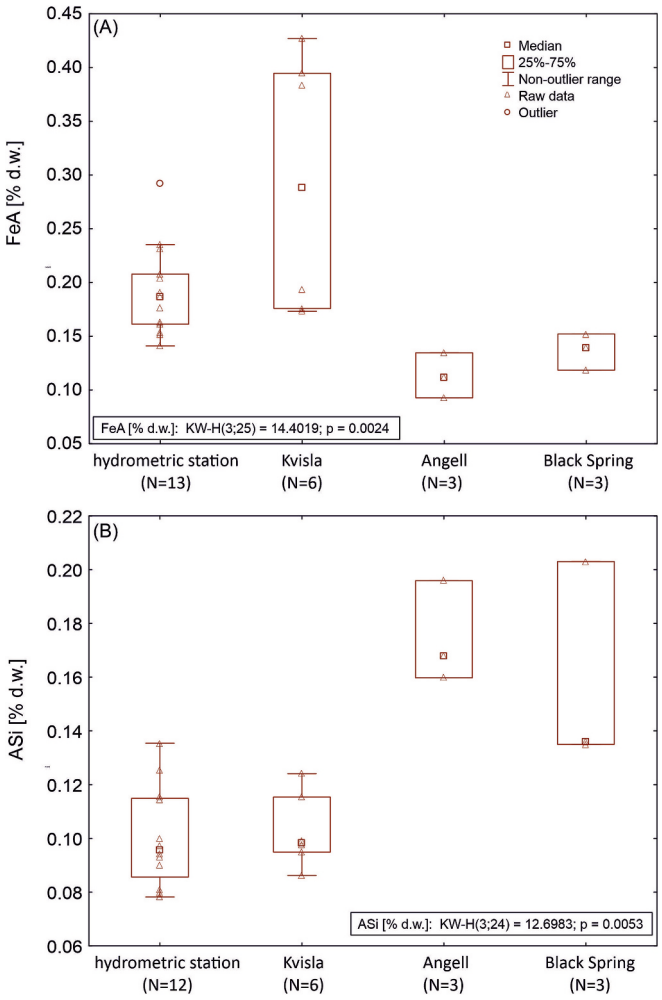

Fig. 6. Spatial distribution of sediment-bound nutrients extracted form samples collected in the catchment of Werenskioldbreen (minor outflows: S1 Angell outflow and S4 Black spring, S2 Kvisla channelized outflow, S3 hydrometric station, Fig. 1). A) ascorbic iron (FeA), B) amorphous silicate (ASi). In boxes, Kruskal-Wallis test shows a significant difference between sites for both plots.

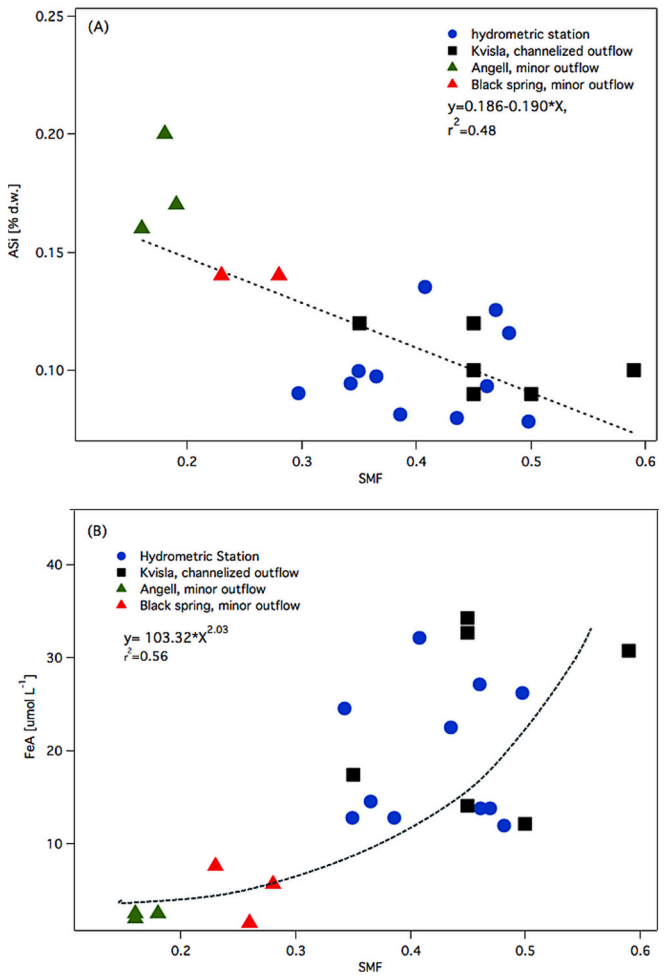

Fig. 7. Relationship between sediment-bound A) amorphous silica, ASi, B) ascorbate iron FeA and sulfate mass fraction (SMF) for all data points.

2016) and FeA in iceberg sediment sourced from glaciers underlain by metasedimentary rocks in Svalbard have a range of values similar to S1, S3 and S4, but lower than S2 (Hopwood et al., 2017; Raiswell et al., 2016).

The spatial distribution of DSi, ASi and P appears to be more influenced by bedrock geology than meltwater/sediment residence times under the glacier. Higher concentrations of both DSi and ASi were observed in the minor subglacial outflows (S1 and S4), which are partly underlain by silicate-rich bedrock (Fig. 8). Similarly, the phosphorous content was higher in the sediments from these outflows, compared with channelised outflow (S2) and hydrometric station (S3; Table 4). These findings suggest that geological differences appear to be more important than meltwater residence time. Elevated concentration of sediment-bound P in S1 links well with occurrence of phosphorous-bearing minerals (e.g., apatite) associated with biotite-rich rocks in the southern part of proglacial zone (Czerny et al., 1992b).

DSi (9.2 μM) and ASi (0.12 % d.w.) from all sites in Werenskioldbreen were 240 % and 20 % higher compared to other sites in Svalbard (Hatton et al., 2019b; Hodson et al., 2000). For just the minor outflows (S1 and S4) draining silicate-rich bedrock, DSi and ASi (10.7 uM and 0.17 % d.w., respectively) were even higher, by up to ~250 % and ~ 70 % respectively (Hatton et al., 2019b; Hodson et al., 2000). However, meltwaters from glacierised basins outside of Svalbard have been found to have higher silicon (and phosphorous) concentrations by the factor of ~2 or more (Hatton et al., 2019a; Hawkings et al., 2016; Hawkings et al., 2017; Hodson et al., 2004; Pryer et al., 2020). DSi, ASi, and P in Werenskioldbreen meltwaters therefore appear to be strongly controlled more by the silicate rich lithology (e.g., amphibolite) rather than meltwater residence time under subglacial drainage.

5.3. *Sediment-bound mass fluxes in glaciers outside ice sheets*

Yields of sediment-bound highly reactive iron (FeA + FeD; 2.3 10^3 kg km^{-2} yr^{-1}, Table 1) from Werenskioldbreen are similar to ice sheets. Specific yields of FeA (Fig. 9) are similar to glacierised basins from Chilean Patagonia (0.97 10^3 kg km^{-2} yr^{-1} (Pryer et al., 2020)) but lower than a large catchment of the Greenland Ice Sheet (5.8 10^3 kg km^{-2} yr^{-1} (Hawkings et al., 2014)). For seasons with higher runoff (e.g., 2008, 2012 (Łepkowska and Stachnik, 2018; Majchrowska et al., 2015)), FeA yields from Werenskioldbreen might exceed values observed in Greenland by 50 % if FeA concentrations are scalable (Table A.4). Notably, specific runoff for 2008 and 2012 (1.91 m and 2.24 m, respectively (Majchrowska et al., 2015) was ~50 % of that observed in the Greenland study. Similarly, for glacierised basins (>10 % glacier cover) in Patagonia, high specific runoff resulted in high sediment-bound iron mass fluxes. This shows that both higher specific glacier meltwater runoff and fluvioglacial erosion of susceptible bedrock (e.g., schist in Werenskioldbreen) can lead to high mass fluxes of FeA and FeD. High meltwater supply is likely to enhance glacial fluvial erosion (Hallet et al., 1996; Łepkowska and Stachnik, 2018), and elevate the mass flux

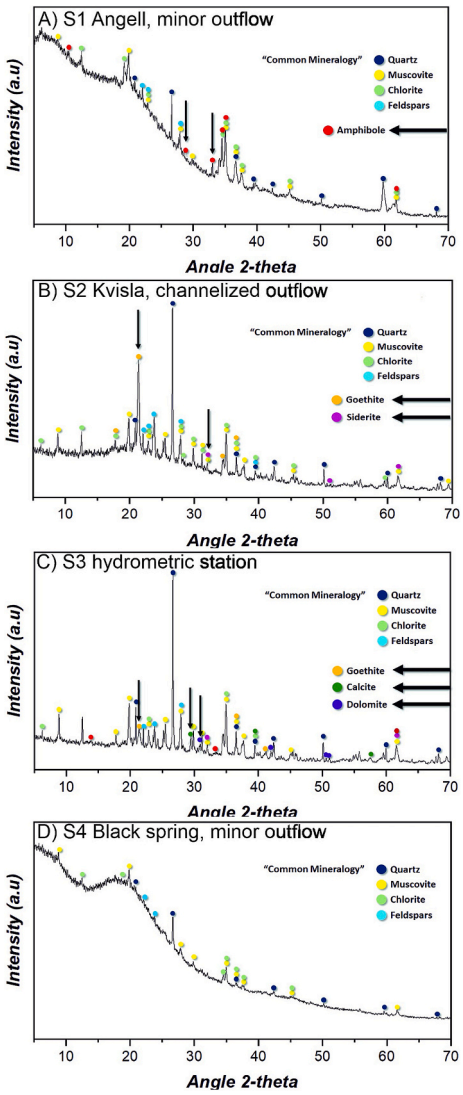

Fig. 8. The X-ray diffraction patterns for samples collected from: A) S1 Angell minor outflow, B) S2 Kvisla channelized outflow, C) S3 hydrometric station, D) S4 Black spring minor outflow.

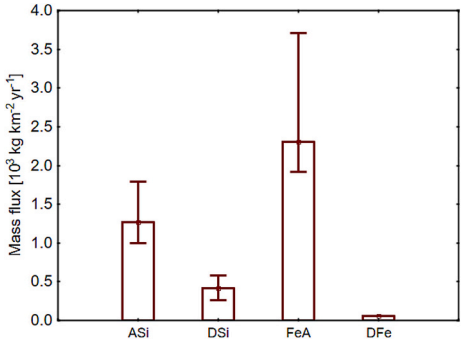

Fig. 9. Sediment-bound (FeA, ASi) and dissolved (DSi, DFe) nutrients mass fluxes at the hydrometric station (S3) in the catchment of Werenskioldbreen in summer 2017. Concentrations of dissolved Fe (DFe) are median values from Stachnik et al. (2019).

of sediment-bound nutrients. Conversely, a transition of the hydrological regime from glacier melt to nival-dominated in the future could lead to a decrease in catchment-suspended sediment concentration and yield (Brahney et al., 2021), leading to lower FeA and FeD mass fluxes unless other biogeochemical processes increase the % d.w. concentration.

This study shows that yields of ASi (on average 1.3 10^3 kg km^{-2} yr^{-1}) from high Arctic glaciers are three times higher than DSi. Earlier studies showed similarly low DSi yields in Svalbard (Hodgkins et al., 1997; Hodson et al., 2002), and ASi yields were in the range of values observed at glacierised catchments situated outside Greenland Ice Sheet (e.g. 1.67 ± 0.99 10^3 kg km^{-2} yr^{-1} for Patagonia) (Pryer et al., 2020). Mass fluxes of SSC, which are more than one order of magnitude higher than Patagonian catchments, are the key driver of ASi mass flux here. The low chemical weathering of silicates compared with other basins (Tables 1, 3) (Torres et al., 2014; Wadham et al., 2010b), as evidenced by lower concentrations of DSi and ASi, and geochemical indices (e.g., (Ca_{carb} + Mg_{carb}):(Ca_{sil} + Mg_{sil} + Na_{sil} + K_{sil}), Mg_{carb}:Na_{sil}, Ca_{carb}:Na_{sil}), (Torres et al., 2014; Wadham et al., 2010b), limits the overall Si fluxes from Werenskioldbreen.

The early stages of glacier recession likely facilitate FeA transport via physical and chemical erosion of susceptible bedrock and high resultant sediment mass fluxes to downstream ecosystems. The rate of glacier erosion is higher for metasedimentary rocks, such as those that underlie Werenskioldbreen, than for igneous rock (e.g. acidic plutonic rock (Crompton and Flowers, 2016; Pryer et al., 2020). The weathering of sedimentary rocks in the Mackenzie River basin has already been found to be important in delivering riverine labile iron to the Arctic Ocean (Larkin et al., 2021). As most of studies dealing with FeA yields were obtained for catchments with igneous bedrock geology, FeA yields from glaciers may be higher than previously believed. The share of metamorphic bedrock is ~13 % of land surface - higher than plutonic and volcanic bedrock (Hartmann and Moosdorf, 2012). This makes areas underlain by metamorphic rock an important missing component of FeA export to the coastal ocean.

5.4. Future changes affecting sediment-bound nutrient mass fluxes

Our study area displays relatively large spatial differences in chemical weathering and associated formation of sediment-bound FeA and ASi in subglacial drainage systems. Future export of nutrients from glacierised catchments will likely be the product of multiple variables, including bedrock lithology, specific runoff, drainage system changes, and water residence time. The strong spatial variation in chemical weathering at Werenskioldbreen indicates that bedrock lithology controls the geochemical processes supplying FeA and ASi, along with high specific runoff facilitating the transport of the weathering products (as per the discussion above). Sulphide oxidation producing FeA (and perhaps FeD over longer time periods) appears to be more important in drainage systems dominated by major subglacial channels, compared to ASi generated via silicate weathering. Sulphuric acid from sulphide oxidation is a potential driver of silicate weathering (Wadham et al., 2010b), but this process appears to be of lower importance at minor outflows (see details in section 5.2).

In addition to lithology, the residence time of water, which is likely higher in the main channelised outflow (S2; (Piechota et al., 2012; Stachniak et al., 2024; Stachniak et al., 2022)), appears to enhance solute contribution from sulphide oxidation (Kemeny et al., 2021). The drainage system beneath polythermal glaciers is dynamic (Stachnik et al., 2016; Wadham et al., 2010a) leading to potential changes in solute and sediment sourcing area and, therefore, bedrock lithology prone to chemical weathering processes. Future changes in the intensity of glacier melt, including high-magnitude ablation events (rain or glacier melt-inducted (Roy et al., 2024), will likely increase the chances of drainage system reconfiguration. In turn, sediment-bound nutrient transport associated with the alteration of chemical weathering may also change.

Glaciers outside of ice sheets appear to mobilise large quantities of FeA and ASi, potentially making them important in the wider carbon cycle via increase in primary and/or secondary production and carbon

burial. Our study shows that Fe supply from glaciers to coastal regions of the High Arctic is likely to be high with potential consequences for marine elemental inventories and carbon burial (Cui et al., 2017; Faust et al., 2021; Larkin et al., 2021; Salvadõ et al., 2015) (Fig. A.6). The delivery of labile sediment-bound Fe had already been shown to enhance benthic nutrient cycling (e.g., Fe, Mn) with potential remobilisation of Fe into the water column (Henkel et al., 2018; Herbert et al., 2021; Laufer-Meiser et al., 2020). FeA and FeD also facilitate deposition and burial of organic matter via mineral protection which could lead to more effective carbon burial in coastal (Salvadõ et al., 2015; Shields et al., 2016) and lacustrine sediments (Nitzsche et al., 2022). As long as the hydrological regime is dominated by glacier melt, rivers in polar regions will likely continue to supply FeA rich suspended sediments to downstream ecosystems.

6. Conclusions

Our study shows that glacierised catchments situated outside of ice sheets supply downstream ecosystems with reactive and bioavailable iron species. The yields of sediment-bound FeA and FeD were in the range of values observed for the Greenland Ice Sheet and are the result of high sediment erosion rates and subglacial geochemical weathering. Conversely, silicate weathering associated mass fluxes of ASi and DSi were in range of other valley glacier basins (e.g. Patagonia, Svalbard), but much lower than for Greenland. Yields of sediment-bound P was much lower than other glacierised basins where similar data is available.

High spatial variability of subglacial weathering processes within the catchment causes differences in sediment-bound and dissolved nutrient release into the proglacial zone of Werenskioldbreen. Within a single catchment, sediment-bound nutrient content can change due to a gradient of sulphide oxidation coupled with carbonate dissolution (high FeA, low ASi/DSi) dominated subglacial weathering to silicate-mineral dominated weathering (high DSi/ASi, low FeA), showing a close relationship to bedrock lithology. In geologically diverse glacial catchments like those in Svalbard, the pattern of subglacial drainage will likely impact the delivery of sediment-bound nutrients.

CRediT authorship contribution statement

Lukasz Stachnik: Writing – original draft, Visualization, Supervision, Data curation, Conceptualization. **Jon Hawkings:** Writing – original draft, Methodology, Investigation, Data curation. **Andrea Spolaor:** Visualization, Methodology, Data curation. **Katarzyna Stachniak:** Writing – original draft, Visualization, Methodology, Investigation. **Dariusz Ignatiuk:** Supervision, Project administration, Methodology, Funding acquisition, Data curation. **Sławomir Sitek:** Methodology, Investigation, Data curation. **Krzysztof Janik:** Investigation, Data curation. **Elżbieta Łepkowska:** Methodology, Investigation, Data curation. **Francois Burgay:** Methodology, Investigation, Data curation. **Marcin Daniel Syczewski:** Writing – original draft, Visualization, Data curation. **Delia Segato:** Visualization, Software, Methodology. **Pablo Forjanes:** Writing – original draft, Visualization, Methodology, Data curation. **Liane G. Benning:** Writing – original draft, Supervision, Methodology, Conceptualization.

Declaration of Competing Interest

The authors declare that they have no known competing financial interests or personal relationships that could have appeared to influence the work reported in this paper.

Acknowledgement

This study is a contribution to the Polish National Science Centre project FLOURISH (SONATA funding scheme, award No. UMO-2021/43/D/ST10/00687) and RAW (GRIEG-1 funding scheme, award No. UMO-2019/34/H/ST10/00504). ŁS was supported from the Bekker Programme (award no. BPN/BEK/2021/1/00431) at the Polish National Agency for Scientific Exchange. JH was supported by the US National Science Foundation project MEGA, award number 2232980. PF and LGB acknowledge the financial support from the Helmholtz Recruiting Initiative grant no. I-044-16-0. We would like to thank Jade Hatton for help during laboratory analyses. This project has received funding from the European Union's Horizon 2020 research and innovation Transnational Access programme EXCITE under grant agreement No 101005611. ŁS acknowledges funding for their transnational Access (TNA id: EXCITE_TNA_C2_2022_008) for research conducted at the Potsdam Imaging and Spectral Analyses (PISA) facility at the GFZ, Helmholtz Centre for Geosciences, Potsdam Germany. KS, DI, SS, KJ, EL carried out this study as part of scientific activity of the Centre for Polar Studies (University of Silesia in Katowice) with the use of research and logistic equipment (monitoring and measuring equipment, sensors, multiple AWS, GNSS receivers, snowmobiles and other supporting equipment) of the Polar Laboratory of the University of Silesia in Katowice. We sincerely thank the two anonymous reviewers for their valuable feedback, which significantly helped improve the quality and clarity of our manuscript.

Appendix A. Supplementary data

Supplementary data to this article can be found online at https://doi.org/10.1016/j.chemgeo.2025.122940.

Data availability

Data used in this study are available at Zenodo (https://zenodo.org/records/10650475).

References

Anderson, S.P., 2005. Glaciers show direct linkage between erosion rate and chemical weathering fluxes. Geomorphology 67 (1–2), 147–157.
Bhatia, M.P., et al., 2013. Organic carbon export from the Greenland ice sheet. Geochim. Cosmochim. Acta 109, 329–344.
Bosson, J.B., et al., 2023. Future emergence of new ecosystems caused by glacial retreat. Nature 620 (7974), 562–569.
Brahney, J., et al., 2021. Glacier recession alters stream water quality characteristics facilitating bloom formation in the benthic diatom Didymosphenia geminata. Sci. Total Environ. 764, 142856.
Bukowska-Jania, E., 2003. The role of glacier systems in the migration of calcium carbonate in the natural environment (with particular reference to Svalbard and the late-glacial areas in NW Poland). In: Prace Naukowe Uniwersytetu Śląskiego, 2103, Katowice, Poland, 247 pp.
Bukowska-Jania, E., 2007. The role of glacier system in migration of calcium carbonate on Svalbard. Polish Polar Res. 28 (2), 137–155.
Chillrud, S.N., Pedrozo, F.L., Temporetti, P.F., Planas, H.F., Froelich, P.N., 1994. Chemical weathering of phosphate and germanium in glacial meltwater streams: Effects of subglacial pyrite oxidation. Limnol. Oceanogr. 39 (5), 1130–1140.
Ciężkowski, W., Głowacki, T., Grudzińska, K., Kasza, D., Zagożdżon, P., 2018. Front of the Werenskiold Glacier (Svalbard) – changes in years 1957–2013. EPJ Web Conf. 29, 00030.
Conley, D.J., 1998. An interlaboratory comparison for the measurement of biogenic silica in sediments. Mar. Chem. 63 (1–2), 39–48.
Cooper, R.J., Wadham, J.L., Tranter, M., Hodgkins, R., Peters, N.E., 2002. Groundwater hydrochemistry in the active layer of the proglacial zone, Finsterwalderbreen, Svalbard. J. Hydrol. 269 (3–4), 208–223.
Crompton, J.W., Flowers, G.E., 2016. Correlations of suspended sediment size with bedrock lithology and glacier dynamics. Ann. Glaciol. 57 (72), 142–150.
Crompton, J.W., Flowers, G.E., Kirste, D., Hagedorn, B., Sharp, M.J., 2015. Clay mineral precipitation and low silica in glacier meltwaters explored through reaction-path modelling. J. Glaciol. 61 (230), 1061–1078.
Cui, X., et al., 2017. Carbon Dynamics along a Temperate Fjord-Head Delta: Linkages with Carbon Burial in Fjords. J. Geophys. Res. Biogeosci. 122 (12), 3419–3430.
Czerny, J., Kieres, A., Manecki, M., Rajchel, J., 1992a. Geological Map of the SW Part of Wedel-Jarlsberg Land, Spitsbergen. Institute of Geology and Mineral Deposits, University of Mining and Metallurgy, Kraków, Poland.
Czerny, J., Lipień, G., Manecki, A., Piestrzyński, A., 1992b. Geology and ore-mineralization of the Hecla Hoek Succession (Precambrian) in front of Werenskioldbreen, South Spitsbergen. Studia Geol. Polonica 98, 67–113.
Dallmann, W.K., Elvevold, S., 2015. Chapter 7. Bedrock geology. In: Dallmann, W.K. (Ed.), Geoscience atlas of Svalbard. Norsk Polarinstitutt, pp. 133–174.

Decaux, L., Grabiec, M., Ignatiuk, D., Jania, J., 2019. Role of discrete water recharge from supraglacial drainage systems in modeling patterns of subglacial conduits in Svalbard glaciers. Cryosphere 13 (3), 735–752. https://doi.org/10.5194/tc-13-735-2019.
DeMaster, D.J., 1981. The Supply and Accumulation of Silica in the Marine-Environment. Geochim. Cosmochim. Acta 45 (10), 1715–1732.
Deuerling, K.M., Martin, J.B., Martin, E.E., Scribner, C.A., 2018. Hydrologic exchange and chemical weathering in a proglacial watershed near Kangerlussuaq, West Greenland. J. Hydrol. 556, 220–232.
Dorich, R.A., Nelson, D.W., Sommers, L.E., 1985. Estimating Algal Available Phosphorus in Suspended Sediments by Chemical Extraction. J. Environ. Qual. 14 (3), 400–405.
Eiriksdottir, E.S., Gislason, S.R., Oelkers, E.H., 2015. Direct evidence of the feedback between climate and nutrient, major, and trace element transport to the oceans. Geochim. Cosmochim. Acta 166, 249–266.
Faust, J.C., et al., 2021. Millennial scale persistence of organic carbon bound to iron in Arctic marine sediments. Nat. Commun. 12 (1).
Follett, E.A.C., McHardy, W.J., Mitchell, B.D., Smith, B.F.L., 1965. Chemical dissolution techniques in the study of soil clays: part I. Clay Miner. 6, 23–34.
Föllmi, K.B., Hosein, R., Arn, K., Steinmann, P., 2009. Weathering and the mobility of phosphorus in the catchments and forefields of the Rhône and Oberaar glaciers, Central Switzerland: Implications for the global phosphorus cycle on glacial-interglacial timescales. Geochim. Cosmochim. Acta 73 (8), 2252–2282.
Frings, P.J., Clymans, W., Conley, D.J., 2014. Amorphous silica transport in the Ganges basin: Implications for Si delivery to the oceans. Geochem. Earth's Surf. Ges-10 10, 271–274.
Gaillardet, J., Dupré, B., Louvat, P., Allègre, C.J., 1999. Global silicate weathering and CO2 consumption rates deduced from the chemistry of large rivers. Chem. Geol. 159 (1), 3–30.
Gassman, P.W., Reyes, M.R., Green, C.H., Arnold, J.G., 2007. The Soil and Water Assessment Tool: Historical Development, applications, and Future Research Directions. Trans. ASABE 50 (4), 1211–1250.
Gibs, J., Wilde, F.D., Heckathorn, H.A., 2007. Use of multiparameter instruments for routine field measurements (ver 1.1). In: USGS (Ed.), U.S. Geological Survey Techniques of Water-Resources Investigations, pp. 1–48.
Grabiec, M., 2017. Stan i współczesne zmiany systemów lodowcowych południowego Spitsbergenu w świetle badań metodami radarowym. The state and contemporary changes of the glacial systems in southern Spitsbergen in the light of the radar methods. In: Prace Naukowe Uniwersytetu Śląskiego w Katowicach, 3536. Wydawnictwo Uniwersytetu Śląskiego, Katowice, p. 328.
Graly, J.A., Humphrey, N.F., Harper, J.T., 2016. Chemical depletion of sediment under the Greenland Ice Sheet. Earth Surf. Process. Landf. 41 (13), 1922–1936.
Hagen, J.O., Liestøl, O., Roland, E., Jørgensen, T., 1993. Glacier Atlas of Svalbard and Jan Mayen, Meddelelser Nr. 129. Norsk Polarinstitutt, Oslo, 166 pp.
Hallet, B., Hunter, L., Bogen, J., 1996. Rates of erosion and sediment evacuation by glaciers: A review of field data and their implications. Glob. Planet. Chang. 12 (1–4), 213–235.
Harland, W.B., 1997. The Geology of Svalbard. Geological Society Memoir, No. 17. Geological Society of London, 521 pp.
Hartmann, J., Moosdorf, N., 2012. The new global lithological map database GLiM: A representation of rock properties at the Earth surface. Geochem. Geophys. Geosyst. 13 (12).
Hatton, J.E., et al., 2019a. Investigation of subglacial weathering under the Greenland Ice Sheet using silicon isotopes. Geochim. Cosmochim. Acta 247, 191–206.
Hatton, J.E., et al., 2019b. Silicon isotopes in Arctic and sub-Arctic glacial meltwaters: the role of subglacial weathering in the silicon cycle. Proc. Royal Soc. A Math. Phys. Eng. Sci. 475 (2228), 20190098.
Hawkings, J., et al., 2016. The Greenland Ice Sheet as a hotspot of phosphorus weathering and export in the Arctic. Glob. Biogeochem. Cycles 30, 1–20.
Hawkings, J., et al., 2018a. Biolabile ferrous iron bearing nanoparticles in glacial sediments. Earth Planet. Sci. Lett. 493, 92–101.
Hawkings, J.R., et al., 2014. Ice sheets as a significant source of highly reactive nanoparticulate iron to the oceans. Nat. Commun. 5, 1–8.
Hawkings, J.R., et al., 2017. Ice sheets as a missing source of silica to the polar oceans. Nat. Commun. 8, 14198.
Hawkings, J.R., et al., 2018b. The silicon cycle impacted by past ice sheets. Nat. Commun. 9 (1), 3210.
Hedley, M.J., Stewart, J.W.B., Chauhan, B.S., 1982. Changes in Inorganic and Organic Soil-Phosphorus Fractions Induced by Cultivation Practices and by Laboratory Incubations. Soil Sci. Soc. Am. J. 46 (5), 970–976.
Henkel, S., Kasten, S., Hartmann, J.F., Silva-Busso, A., Staubwasser, M., 2018. Iron cycling and stable Fe isotope fractionation in Antarctic shelf sediments, King George Island. Geochim. Cosmochim. Acta 237, 320–338.
Herbert, L.C., et al., 2021. Benthic iron flux influenced by climate-sensitive interplay between organic carbon availability and sedimentation rate in Arctic fjords. Limnol. Oceanogr. 66 (9), 3374–3392.
Hodgkins, R., Tranter, M., Dowdeswell, J.A., 1997. Solute provenance, transport and denudation in a High Arctic glacierized catchment. Hydrol. Process. 11 (14), 1813–1832.
Hodson, A., Tranter, M., Vatne, G., 2000. Contemporary rates of chemical denudation and atmospheric CO_2 sequestration in glacier basins: an arctic perspective. Earth Surf. Process. Landf. 25 (13), 1447–1471.
Hodson, A., Tranter, M., Gurnell, A., Clark, M., Hagen, J.O., 2002. The hydrochemistry of Bayelva, a high Arctic proglacial stream in Svalbard. J. Hydrol. 257 (1–4), 91–114.
Hodson, A., Mumford, P., Lister, D., 2004. Suspended sediment and phosphorous in proglacial rivers: Bioavailability and potential impacts upon the P status of ice-marginal receiving waters. Hydrol. Process. 18, 2409–2422.
Hodson, A.J., et al., 2017. Climatically sensitive transfer of iron to maritime Antarctic ecosystem by surface runoff. Nat. Commun. 8, 1–7.
Holt, A., et al., 2021. The evolution of stream dissolved organic matter composition following glacier retreat in coastal watersheds of Southeast Alaska. Biogeochemistry 164, 99–116.
Hood, E., Berner, L., 2009. Effects of changing glacial coverage on the physical and biogeochemical properties of coastal streams in southeastern Alaska. J. Geophys. Res. Biogeosci. 114 (G3).
Hood, E., Battin, T.J., Fellman, J., O'Neel, S., Spencer, R.G.M., 2015. Storage and release of organic carbon from glaciers and ice sheets. Nat. Geosci. 8, 91.
Hopwood, M.J., Cantoni, C., Clarke, J.S., Cozzi, S., Achterberg, E.P., 2017. The heterogeneous nature of Fe delivery from melting icebergs. Geochem. Persp. Lett. 3, 200–209.
Ignatiuk, D., et al., 2022. A decade of glaciological and meteorological observations in the Arctic (Werenskioldbreen, Svalbard). Earth Syst. Sci. Data 14 (5), 2487–2500.
IPCC, 2019. Summary for policymakers. In: Pörtner, H.O., et al. (Eds.), IPCC special Report on the Ocean and Cryosphere in a Changing Climate.
Jania, J., 1988. Klasyfikacja i cechy morfometryczne lodowców otoczenia Hornsundu. In: Spitsbergen, Wyprawy Polarne Uniwersytetu Śląskiego 1980-1984, pp. 12–47.
Kabala, C., Zapart, J., 2012. Initial soil development and carbon accumulation on moraines of the rapidly retreating Werenskiold Glacier, SW Spitsbergen, Svalbard archipelago. Geoderma 175-176, 9–20.
Kemeny, P.C., et al., 2021. Sulfate sulfur isotopes and major ion chemistry reveal that pyrite oxidation counteracts CO2 drawdown from silicate weathering in the Langtang-Trisuli-Narayani River system, Nepal Himalaya. Geochim. Cosmochim. Acta 294, 43–69.
Kieres, A., Piestrzyński, A., 1992. Ore-mineralization of the Hecla Hoek Succession (Precambrian) around Werenskioldbreen, South Spitsbergen. Studia Geol. Polonica 98, 115–151.
Koffman, B.G., et al., 2021. Glacial Dust Surpasses both Volcanic Ash and Desert Dust in its Iron Fertilization potential. Glob. Biogeochem. Cycles 35 (4).
Kristiansen, S.M., et al., 2013. Geochemistry of groundwater in front of a warm-based glacier in Southeast Greenland. Geogr. Ann. Ser. B 95 (2), 97–108.
Kwaśniak-Kominek, M., Manecki, M., Rzepa, G., Płonka, A.M., Górniak, D., 2016. Weathering in a regolith on the Werenskioldbreen forefield (SW spitsbergen): Modelling of pore water chemistry. Ann. Soc. Geol. Pol. 86 (3), 249–264.
Larkin, C.S., et al., 2021. Constraints on the source of reactive phases in sediment from a major Arctic river using neodymium isotopes. Earth Planet. Sci. Lett. 565, 116933.
Laufer-Meiser, K., et al., 2020. Bioavailable iron produced through benthic cycling in glaciated Arctic fjords (Svalbard). Nat. Commun. 12 (1349).
Łepkowska, E., Stachnik, Ł., 2018. Which Drivers Control the Suspended Sediment Flux in a High Arctic Glacierized Basin (Werenskioldbreen, Spitsbergen)? Water 10 (10), 1408.
Liu, W., et al., 2023. Lithological and glacial controls on sulfide weathering and the associated CO2 budgets in the Tibetan Plateau: New constraints from small catchments. Geochim. Cosmochim. Acta. 343, 341–352.
Majchrowska, E., Ignatiuk, D., Jania, J., Marszałek, H., Wąsik, M., 2015. Seasonal and interannual variability in runoff from the Werenskioldbreen catchment Spitsbergen. Polish Polar Res. 36 (3), 197–224.
Majka, J., Mazur, S., Manecki, M., Czerny, J., Holm, D.K., 2008. Late Neoproterozoic amphibolite-facies metamorphism of a pre-Caledonian basement block in southwest Wedel Jarlsberg Land, Spitsbergen: new evidence from U–Th–Pb dating of monazite. Geol. Mag. 145 (6), 822–830.
Milner, A.M., et al., 2017. Glacier shrinkage driving global changes in downstream systems. Proc. Natl. Acad. Sci. 114 (37), 9770–9778.
Mitchell, A.C., Brown, G.H., 2007. Diurnal hydrological – physicochemical controls and sampling methods for minor and trace elements in an Alpine glacial hydrological system. J. Hydrol. 332 (1–2), 123–143.
Mitchell, A.C., Lafrenière, M.J., Skidmore, M.L., Boyd, E.S., 2013. Influence of bedrock mineral composition on microbial diversity in a subglacial environment. Geology 41 (8), 855–858.
Mueller, D.R., Vincent, W.F., Pollard, W., Fritsen, C., 2001. Glacial cryoconite ecosystems: A bipolar comparison of algal communities and habitats. Nova Hedwigia 123, 173–197.
Navarro, F.J., et al., 2014. Ice volume estimates from Ground-Penetrating Radar surveys, Wedel Jarlsberg Land Glaciers, Svalbard. Arct. Antarct. Alp. Res. 46 (2), 394–406.
Neitsch, S.L., Arnold, J.G., Kiniry, J.R., Williams, J.R., 2011. Soil and Water Assessment Tool Theoretical Documentation Version 2009. Texas Water Resources Institute, Temple, Texas.
Nitzsche, K.N., Kayler, Z.E., Premke, K., Gessler, A., Wagai, R., 2022. Divergent roles of iron and aluminum in sediment organic matter association at the terrestrial–aquatic interface. Biogeochemistry 157 (3), 355–378.
Pälli, A., Moore, J.C., Jania, J., Kolondra, L., Głowacki, P., 2003. The drainage pattern of Hansbreen and Werenskioldbreen, two polythermal glaciers in Svalbard. Polar Res. 22 (2), 355–371.
Piechota, A.M., Sitek, S., Ignatiuk, D., Piotrowski, J.A., 2012. Reconstructing subglacial drainage of Werenskiold Glacier (SW Spitsbergen) based on numerical modelling. Biuletyn Państwowego Instytutu Geologicznego 451, 191–202.
Poulton, S.W., Raiswell, R., 2002. The Low-temperature Geochemical Cycle of Iron: From Continental Fluxes to Marine Sediment Deposition, p. 302.
Poulton, S.W., Raiswell, R., 2005. Chemical and physical characteristics of iron oxides in riverine and glacial meltwater sediments. Chem. Geol. 218 (3), 203–221.
Pryer, H.V., et al., 2020. The Influence of Glacial Cover on Riverine Silicon and Iron exports in Chilean Patagonia. Glob. Biogeochem. Cycles 34, e2020GB006611.

Raiswell, R., et al., 2006. Contributions from glacially derived sediment to the global iron (oxyhydr)oxide cycle: Implications for iron delivery to the oceans. Geochim. Cosmochim. Acta 70 (11), 2765–2780.
Raiswell, R., Vu, H.P., Brinza, L., Benning, L.G., 2010. The determination of labile Fe in ferrihydrite by ascorbic acid extraction: Methodology, dissolution kinetics and loss of solubility with age and de-watering. Chem. Geol. 278 (1–2), 70–79.
Raiswell, R., et al., 2016. Potentially bioavailable iron delivery by iceberg-hosted sediments and atmospheric dust to the polar oceans. Biogeosciences 13 (13), 3887–3900.
Raiswell, R., et al., 2018. Iron in Glacial Systems: Speciation, Reactivity, Freezing Behavior, and Alteration during Transport. Front. Earth Sci. 6 (222).
Robison, A.L., Deluigi, N., Rolland, C., Manetti, N., Battin, T., 2023. Glacier loss and vegetation expansion alter organic and inorganic carbon dynamics in high-mountain streams. Biogeosciences 20 (12), 2301–2316.
Roy, N., Sen, I.S., Boral, S., Shukla, T., Velu, V., 2024. Isotope hydrograph separation reveals rainfall on the glaciers will enhance ice meltwater discharge to the Himalayan rivers. Water Resour. Res. 60, e2023WR034528. https://doi.org/10.1029/2023WR034528.
Rzepa, G., et al., 2019. Weathering in a regolith on the Werenskioldbreen Glacier forefield (SW Spitsbergen). 2. Speciation of Fe, Mn, Pb, Cu and Zn in the chronosequence. Ann. Soc. Geol. Pol. 89 (3), 317–341.
Salvadó, J.A., et al., 2015. Organic carbon remobilized from thawing permafrost is resequestered by reactive iron on the Eurasian Arctic Shelf. Geophys. Res. Lett. 42 (19), 8122–8130.
Shields, M.R., Bianchi, T.S., Gélinas, Y., Allison, M.A., Twilley, R.R., 2016. Enhanced terrestrial carbon preservation promoted by reactive iron in deltaic sediments. Geophys. Res. Lett. 43 (3), 1149–1157.
Shukla, T., Sen, I.S., Sundriyal, S., 2023. Carbon emissions from emerging glacier-fed Himalayan lakes. Global and Planetary Change 225, 104134.
Shoenfelt, E.M., et al., 2017. High particulate iron(II) content in glacially sourced dusts enhances productivity of a model diatom. Sci. Adv. 3 (6), e1700314.
St. Pierre, K.A., et al., 2019. Proglacial freshwaters are significant and previously unrecognized sinks of atmospheric CO₂. Proc. Natl. Acad. Sci. 116 (36), 17690–17695.
Stachniak, K., Sitek, S., Ignatiuk, D., Jania, J., 2022. Hydrogeological Model of the Forefield Drainage System of Werenskioldbreen, Svalbard. Water 14 (9), 1514.
Stachniak, K., Janik, K., Sitek, S., 2024. Proglacial sediments in High Arctic glacier foreland: A case study of Werenskioldbreen. Svalbard Polish Polar Res. 45 (4), 255–283.
Stachnik, Ł., et al., 2016. Chemical denudation and the role of sulfide oxidation at Werenskioldbreen, Svalbard. J. Hydrol. 538, 177–193.
Stachnik, Ł., et al., 2019. Aluminium in glacial meltwater demonstrates an association with nutrient export (Werenskiöldbreen, Svalbard). Hydrol. Process. 33, 1638–1657.
Stachnik, Ł., et al., 2022. SEM-EDS and water chemistry characteristics at the early stages of glacier recession reveal biogeochemical coupling between proglacial sediments and meltwater. Sci. Total Environ. 835, 155383.
Stibal, M., Tranter, M., Telling, J., Benning, L.G., 2008. Speciation, phase association and potential bioavailability of phosphorus on a Svalbard glacier. Biogeochemistry 90 (1), 1–13.
Sułowicz, S., Bondarczuk, K., Ignatiuk, D., Jania, J.A., Piotrowska-Seget, Z., 2020. Microbial communities from subglacial water of naled ice bodies in the forefield of Werenskioldbreen, Svalbard. Sci. Total Environ. 723, 138025.
Sundriyal, S., Shukla, T., Kang, S., Zhang, Y., Dobhal, D.P., Singh, R., 2024. Controls of lithology and climate over chemical weathering trends: new insights from the precipitation-dominated Dokriani glacier, central Himalaya, India. J. Glacio. 70, e75. https://doi.org/10.1017/jog.2023.108.
Szynkiewicz, A., Modelska, M., Buczyński, S., Borrok, D.M., Merrison, J.P., 2013. The polar sulfur cycle in the Werenskioldbreen, Spitsbergen: possible implications for understanding the deposition of sulfate minerals in the North Polar Region of Mars. Geochim. Cosmochim. Acta 106, 326–343.
Torres, M.A., West, A.J., Li, G., 2014. Sulphide oxidation and carbonate dissolution as a source of CO_2 over geological timescales. Nature 507 (7492), 346–349.
Tranter, M., Wadham, J.L., 2013. Geochemical Weathering in Glacial and Proglacial Environments. Second Edition. Elsevier Inc., Treatise on Geochemistry, pp. 157–173.
Tranter, M., et al., 2002. Geochemical weathering at the bed of Haut glacier d'Arolla, Switzerland - A new model. Hydrol. Process. 16 (5), 959–993.
Vinšová, P., et al., 2022. The Biogeochemical Legacy of Arctic Subglacial Sediments Exposed by Glacier Retreat. Glob. Biogeochem. Cycles 36 (3), e2021GB007126.
Viollier, E., Inglett, P.W., Hunter, K., Roychoudhury, A.N., Van Cappellen, P., 2000. The ferrozine method revisited: Fe(II)/Fe(III) determination in natural waters. Appl. Geochem. 15 (6), 785–790.
Wadham, J.L., et al., 2010a. Hydro-biogeochemical coupling beneath a large polythermal Arctic glacier: Implications for subice sheet biogeochemistry. J. Geophys. Res. F: Earth Surf. 115 (4), F04017.
Wadham, J.L., et al., 2010b. Biogeochemical weathering under ice: size matters. Glob. Biogeochem. Cycles 24 (3), GB3025.
Waychunas, G., Kim, C., Banfield, J., 2005. Nanoparticulate Iron Oxide Minerals in Soils and Sediments: Unique Properties and Contaminant Scavenging Mechanisms. J. Nanopart. Res. 7, 409–433.
Wyatt, N.J., et al., 2023. Phytoplankton responses to dust addition in the Fe–Mn co-limited eastern Pacific sub-Antarctic differ by source region. Proc. Natl. Acad. Sci. 120 (28), e2220111120.
Yde, J.C., et al., 2010. Basal ice microbiology at the margin of the Greenland ice sheet. Ann. Glaciol. 51 (56), 71–79.